Precursors of select GPI-anchored proteins positively regulate GPI biosynthesis under the control of ERAD

Yi-Shi Liu
Jiangnan University
Yicheng Wang
Osaka University https://orcid.org/0000-0001-7789-1938
Xiaoman Zhou
Jiangnan University
LinPei Zhang
Jiangnan University
Ganglong Yang
Jiangnan University
Xiao-Dong Gao
Jiangnan University https://orcid.org/0000-0002-8575-5095
Yoshiko Murakami
Osaka University https://orcid.org/0000-0002-4870-5734
Morihisa Fujita
Jiangnan University https://orcid.org/0000-0002-0344-2408
Taroh Kinoshita (tkinoshi@biken.osaka-u.ac.jp)
Osaka University https://orcid.org/0000-0001-7166-7257

Article

Keywords: glycosylphosphatidylinositol, endoplasmic reticulum associated degradation, CD55 precursor

Posted Date: November 11th, 2021

DOI: https://doi.org/10.21203/rs.3.rs-998556/v1

Abstract

We previously reported that glycosylphosphatidylinositol (GPI) biosynthesis is regulated by endoplasmic reticulum associated degradation (ERAD); however, the underlying mechanistic basis remains unclear. Based on a genome-wide CRISPR–Cas9 screen, we show that a widely expressed GPI-anchored protein CD55 precursor and ER-resident ARV1 together upregulate GPI biosynthesis under ERAD-deficient conditions. In cells defective in GPI transamidase, GPI-anchored protein precursors fail to obtain GPI, remaining the uncleaved GPI-attachment signal at the C-termini. We show that ERAD deficiency causes accumulation of the CD55 precursor, which in turn upregulates GPI biosynthesis, where the GPI-attachment signal peptide is the active element. Among the 32 GPI-anchored proteins tested, only the GPI-attachment signal peptides of CD55 and CD48 enhance GPI biosynthesis. ARV1 is essential for the GPI upregulation by CD55 precursor. Our data demonstrate an ARV1-dependent regulatory connection between GPI biosynthesis and precursors of select GPI-anchored proteins that are under the control of ERAD.

Introduction

The endoplasmic reticulum (ER) is a specialized eukaryotic organelle for protein synthesis and processing, lipid synthesis, and calcium storage and release [1–3]. Various posttranslational modifications of proteins that reside in or traverse secretory pathways also occur in the ER. For example, N-linked glycans are attached in the ER for efficient folding and proper functions [2,4,5]. Glycosylphosphatidylinositol (GPI) anchoring is one of the conserved posttranslational modifications in eukaryotic cells. More than 150 human proteins have been confirmed as GPI-anchored proteins (GPI-APs) [6,7]. GPIs confer characteristic features to the modified proteins that are essential for embryogenesis, neurogenesis, immune response, and fertilization [8–11]. GPI-APs are biosynthesized in the ER and transported to the cell surface through the Golgi apparatus. The common backbone of GPI, EtNP-6Manα-2Manα-6Manα-4GlcNα-6inositol-phospholipid (where EtNP, Man, and GlcN are ethanolamine phosphate, mannose and glucosamine, respectively), is generated by sequential additions of components to the phosphatidylinositol (PI) moiety [12,13]. Once assembled, GPI is attached to the proteins by GPI transamidase and then undergoes structural remodeling in both glycan and lipid portions [14–16]. The structural variations of GPI anchors are introduced by modification of the core by side chains. The first, α1,6-linked mannose, is often modified by β1,4-linked N-acetylgalactosamine (GalNAc) by PGAP4 [17]. The GalNAc side chain can be further modified by β1,3 galactose (Gal) and then with sialic acid [17,18]. Sialic acid in the GPI side chain of prion proteins, α2-3-linked N-acetylneuraminic acid [18], affects process of prion disease progression [18] ; however, the biological roles of the GPI side chains in various GPI-APs are largely unknown.

The initial GPI identified is a type of glycolipid that anchors various proteins on the cell membrane. In certain parasites, nonprotein-linked GPIs (free GPIs) exist on the membrane [19–21]. In addition, recent works have indicated that free GPIs are also found in some tissues and cell types in mammals [22–25]. The

T5-4E10 monoclonal antibody (T5 mAb), originally established against free GPI from the parasite *Toxoplasma gondii*, recognizes a GalNAc side chain only when GalNAc is at the nonreducing end [20,21]. We found that the T5 mAb also recognizes mammalian free GPIs with a GalNAc side chain and that when the GalNAc side chain is modified by Gal, the T5 mAb no longer binds [17] (Fig. 1a). We also found that when GPI transamidase is defective, GPIs are expressed as free GPIs on the cell surface [22]. Nevertheless, in HEK293 cells, GPI transamidase defects caused by knockout (KO) of PIGS, one of the GPI transamidase components, did not induce positive T5 mAb staining [26], because all the GalNAc side chains were modified by Gal. This phenomenon allowed us to perform genome-wide CRISPR screening for genes involved in GPI side-chain galactosylation. Among genes with KO resulting in positive T5 mAb staining of PIGS-KO HEK293 cells, we identified B3GALT4, which transfers Gal to the GalNAc side chain [26]. In the same screening, we found that KO of ER-associated degradation (ERAD) pathway genes, such as HRD1, UBE2J1 and UBE2G2, caused positive T5 mAb staining and demonstrated that GPI biosynthesis was upregulated in ERAD-defective PIGS-KO cells, so that the amount of free GPI surpassed the galactosylation capacity of the cells resulting in positive staining of the cell by T5 mAb [26].

ERAD plays a critical role in proteostasis under normal or stress conditions. Proteins that fail to fold or assemble are recognized by chaperones and lectins, transferred to membrane-integral adaptors and retrotranslocated through E3 ubiquitin ligases, followed by ubiquitination for cytosolic proteasomal degradation [27–30]. The ERAD system consists of several parallel pathways, ERAD-L, ERAD-M, and ERAD-C, handling the substrate proteins in the ER lumen, ER membrane, and ER cytoplasmic surface, respectively [28,31–34]. Various E3 ligases, including HRD1, GP78, TRC8, and MARCH6, are utilized in these pathways [28,30]. HRD1 is the best characterized and the major retrotranslocation component for luminal ERAD-L substrates [35,36]. Both in vitro and in vivo studies have revealed that multi-membrane spanning HRD1 serves as a channel for luminal ERAD-L substrates. HRD1 recognizes a variety of substrates to maintain ER homeostasis [35–37].

To reveal the mechanism by which the ERAD pathway regulates GPI biosynthesis, we performed genome-wide CRISPR screening to identify factors involved in GPI biosynthesis upregulation under the control of the ERAD pathway. We identified two GPI precursor proteins, CD55 (also known as complement decay-accelerating factor, DAF) and CD48, which are recognized as HRD1-dependent ERAD-L substrates and act as positive regulators of GPI biosynthesis. Our results suggest that GPI biosynthesis is regulated on demand by the status of GPI precursor proteins.

Results

Biosynthesis of GPI is upregulated in ERAD-L deficient cells

As mentioned above, B3GALT4 transfers Gal to the GalNAc side chains of GPI-APs and free GPI [26] (Fig. 1a). As T5 mAb detects the nonmodified GalNAc side chain of free GPI, PIGS-KO cells are T5 mAb staining-negative, whereas PIGS-B3GALT4- double KO (DKO) HEK293 cells become T5 mAb staining-

positive (Fig. 1b). We also found that PIGS-HRD1-DKO cells were strongly stained with the T5 mAb even with intact B3GALT4 (Fig. 1b and 1c), suggesting that the amount of free GPI surpassed the Gal-addition capacity of B3GALT4. GPI transamidase consists of five subunits: PIGS, PIGK, PIGT, PIGU, and GPAA1. To check whether this increase in GPI under HRD1-defective conditions was PIGS KO specific or common among GPI transamidase defects, we knocked out the HRD1 gene in GPI transamidase gene-deficient HEK293 cells and analyzed free GPI levels on the cell surface in bulk populations. Knocking out HRD1 in PIGK-, PIGT-, PIGU-, and GPAA1-KO cells increased T5 mAb staining, as observed in PIGS-HRD1-DKO cells (Fig. 1d), indicating that defects in HRD1 generally increase free GPIs in cells defective in GPI transamidase. We also knocked out HRD1 in SLC35A2 (encoding UDP-galactose transporter necessary for galactosyltransferases) and PIGT double knockout (SLC35A2-PIGT-DKO) HEK293 cells. HRD1 knockout in SLC35A2-PIGT-DKO cells increased T5 mAb staining levels twofold (Fig. 1e and 1f). These results indicated that the ERAD-L pathway suppressed GPI biosynthesis. We hypothesized that there must be positive regulator(s) of GPI biosynthesis, which is controlled by the ERAD-L pathway (Fig. 1g).

Identification of positive regulators of GPI biosynthesis

To identify genes that upregulate GPI biosynthesis when ERAD-L is inactive, we performed a genome-wide CRISPR–Cas9 screen in PIGS-HRD1-DKO HEK293 cells. PIGS-HRD1-DKO cells expressed ~3-fold higher levels of free GPI, as assessed by T5 mAb staining compared with parental PIGS-KO cells, allowing the selection of mutant cells defective in upregulation of GPI biosynthesis. PIGS-HRD1-DKO cells were transduced with lentivirus capable of expressing a human genome-scale CRISPR knockout guide RNA (gRNA) library (GeCKO v2) and Cas9 enzyme. We then cultured the cells for 2 weeks, and cells negatively stained with the T5 mAb were enriched by cell sorting (Fig. 2a). After two rounds of cell sorting and culture, more than half of the cells became negative for T5 mAb staining (Fig. 2b). Genomic DNA was extracted from cells, and the integrated gRNA sequences amplified by PCR were analyzed by deep sequencing. The enrichment of gRNAs was determined by model-based analysis of the genome-wide CRISPR–Cas9 knockout (MAGeCK) method [38]. The screening enriched for genes required for GPI biosynthesis (PIG genes) and dolichol-phosphate mannose (DPM) biosynthesis (DPM1, DPM2, DPM3, SRD54A3, and DHDDS), as expected. CLPTM1L (cleft lip and palate transmembrane protein 1-like protein) was highly enriched in the screening. We recently reported that CLPTM1L is a lipid scramblase involved in GPI biosynthesis [39] (Fig. 2c and Supplementary Fig. 1a). SPPL3, which encodes a membrane-bound aspartic protease that cleaves type-II membrane proteins at the Golgi, was also enriched in the screening. It has been reported that SPPL3 affects the expression of a GPI-AP, CD59, through the regulation of glycosphingolipid biosynthesis [40,41]. Considering that the screen would identify substrates of the ERAD-L pathway, we expanded our attention to other genes encoding ER-localized proteins. Two GPI-related genes, ARV1 and CD55, although they were not highly ranked (ranking #88 and #280, respectively), attracted our attention (Fig. 2c). To validate the screening results, we chose and knocked out five genes, SRD5A3, ARV1, CD55, SPPL3, and CLPTM1L, in PIGS-HRD1-DKO cells. The KO cells were analyzed by staining with T5 mAb. All KO cells showed a clear decrease in T5 mAb staining compared with parental PIGS-HRD1-DKO cells. In particular, T5 mAb staining decreased to nearly background levels

after knocking out ARV1 or CD55 (Fig. 2d and 2e). Decreased T5 mAb staining was restored by overexpression of relevant cDNAs (Supplementary Fig. 1b). When SRD5A3, ARV1, SPPL3, and CLPTM1L were knocked out in HEK293 wild-type cells, the surface CD59, a GPI-AP, was only slightly decreased or unchanged compared with parental wild-type cells (Supplementary Fig. 1c and 1d). These genes were not identified from previous genetic screens using cell surface GPI-APs as reporters. These data suggested that free GPI would be a more sensitive reporter, enabling us to identify more genes involved in GPI biosynthesis.

CD55 precursor regulates GPI biosynthesis under ERAD control

Among the candidate genes identified in the screening, CD55 encodes a GPI-anchored complement regulatory factor that is ubiquitously expressed in the human body. To understand the cellular mechanisms by which knocking out the GPI-AP gene causes a decrease in GPI biosynthesis, we first generated a PIGS-HRD1-CD55-triple KO (TKO) cell line, in which the expression of surface-free GPIs decreased to the background level (Fig. 2d and 3a). When we stably expressed HA-tagged CD55 in the TKO cells, the amounts of surface-free GPIs were restored or even higher than those in PIGS-HRD1-DKO cells (Fig. 3a and 3b). To test whether the change was due to GPI biosynthesis, we metabolically labeled cells with [2-^{3}H] mannose and analyzed radiolabeled GPI mannolipids by thin-layer chromatography. The GPI precursors (H5, H6, H7, H7’ and H8) were decreased by knocking out CD55, whereas they were greatly increased by overexpression of CD55, suggesting that GPI biosynthesis was upregulated by expression of CD55 in PIGS-HRD1-CD55-TKO cells (Fig. 3c).

In normal cells, CD55 protein is synthesized and attached to GPI catalyzed by GPI transamidase in the ER, whereas in PIGS-KO cells, CD55 fails to link to GPI and remains in a precursor form that possesses a GPI attachment signal peptide at the C-terminus. We next analyzed the localization of CD55 in PIGS-HRD1-KO HEK293 cells by immunofluorescence. The precursor of CD55 was mainly colocalized with an ER marker, calnexin (CANX), but only weakly with a Golgi marker, GM130 (Fig. 3d), suggesting that majority of CD55 precursor proteins remain in the ER. GPI-AP precursor proteins that fail to anchor GPI are thought to be degraded through ERAD pathways [42,43]. To validate whether the CD55 precursor was an ERAD substrate, we analyzed endogenous CD55 levels. Western blots revealed specific endogenous immature CD55 bands in PIGS-HRD1-DKO, PIGS-UBE2J1-DKO, and PIGS-UBE2G2-DKO cells (Fig. 3e). In contrast, bands did not appear in PIGS-KO, HRD1-rescued PIGS-HRD1-DKO or PIGS-HRD1-CD55-TKO cells. The protein was also undetectable in PIGS-GP78-DKO cells. The E3 ligase GP78 plays a role in another ERAD pathway for membrane proteins, ERAD-M (Fig. 3e), suggesting that the CD55 precursor is mainly degraded by the HRD1-dependent ERAD-L pathway. We further transiently overexpressed HA-CD55 in PIGS-KO and PIGS-HRD1-DKO cells. The amount of HA-CD55 was much higher when HRD1 was defective (Fig. 3f). To determine the stability of HA-CD55, we treated PIGS-KO and PIGS-HRD1-KO cells with cycloheximide (CHX) to stop new synthesis of proteins. In PIGS-KO cells, CD147, one of the classic ERAD-L substrates, was degraded in a time-dependent manner. HA-CD55 was undetectable under similar conditions. However, both CD147 and HA-CD55 proteins became stable in PIGS-HRD1-DKO cells (Fig. 3g).

These results indicated that the CD55 precursor was a substrate of the HRD1-dependent ERAD pathway and that its accumulation in PIGS-HRD1-DKO cells caused the upregulation of GPI biosynthesis.

To understand the mechanistic basis of GPI biosynthesis upregulation by the CD55 precursor, we performed RNA sequencing (RNA-seq) of samples of parental PIGS-HRD1-DKO, PIGS-HRD1-CD55-TKO, and PIGS-HRD1-CD55-TKO HA-CD55 stably overexpressing cells. Total RNA was extracted and analyzed. The expression profile of GPI biosynthesis-related genes was not significantly affected by CD55 (Supplementary Fig. 2a). To directly test whether PIG genes were involved in the GPI biosynthesis upregulation, we transiently transfected PIG genes or a mixture of DPM-related genes into PIGS-HRD1-CD55-TKO cells, but no effects on these transfected cells were found (Supplementary Fig. 2b). Together, these findings suggested that CD55 did not regulate GPI biosynthesis through changing the protein expression levels of or stabilizing PIG gene-encoded proteins.

Two GPI attachment signal peptides regulate GPI biosynthesis

Mature CD55 (GPI form) contains four short consensus repeats (SCRs), one N-linked glycan between SCR 1 and 2, and a membrane-proximal O-linked polysaccharide rich region (S/T region) [44-46] (Fig. 4a). The CD55 precursor (ER form) is synthesized and translocated into the ER lumen through an N-terminal signal peptide and probably localized in the ER membrane through the hydrophobic region in the C-terminal GPI attachment signal peptide before GPI attachment (Fig. 4a). To determine which part of CD55 is critical for the regulation of GPI biosynthesis, we constructed truncated variants (Fig. 4a) and transiently transfected them into PIGS-HRD1-CD55-TKO cells. Cells expressing CD55 mutants lacking SCR domains or the S/T region efficiently rescued surface-free GPIs (Fig. 4b). However, CD55 lacking a GPI attachment signal (T349–381) could not rescue the expression of free GPIs. A construct only having the 32-amino acid GPI attachment signal (T35–349) also showed no activity, probably due to instability or difficult expression (Fig. 4b-4d). To clarify this issue, we fused the GPI attachment signal of CD55 with GFP protein [GFP-CD55(C)] and transiently overexpressed it in PIGS-HRD1-CD55-TKO cells. Chimera GFP-CD55(C) was expressed well and restored surface-free GPIs (Fig. 4e and 4f), indicating a unique role of the GPI attachment signal of CD55 in regulating GPI biosynthesis.

Considering that more than 150 different human proteins are GPI-APs, we next investigated whether other GPI-AP precursors had the ability to upregulate GPI biosynthesis, similar to CD55. In HEK293 cells, thirteen of 161 GPI-APs were expressed at higher levels than CD55 [47] (Fig. 5a). We then chose five of them (LY6E, GPC4, CD59, CD109, and PRNP) and CD55, which were knocked out by two different gRNAs in PIGS-HRD1-DKO cells. All gene knockouts except CD55 failed to decrease T5 mAb staining (Supplementary Fig. 3a). Conversely, we overexpressed GPI-APs, the expression of which was low, in PIGS-HRD1-CD55-TKO cells (Fig. 5a and Supplementary Fig. 3b). Among the 32 GPI-APs tested, only CD48 efficiently restored the expression of free GPIs (Supplementary Fig. 3b). With the finding that the GPI attachment signal peptide of CD55 regulated GPI biosynthesis, the GPI attachment signal of CD48 was fused with GFP [GFP-CD48(C)], which was expressed in PIGS-HRD1-CD55-TKO cells. The fused protein also restored the expression of free GPIs (Fig. 5b), suggesting that some particular GPI

attachment signals, such as those of CD55 and CD48, were functional in the positive regulation of GPI biosynthesis.

We next asked whether CD48 precursor is a substrate of ERAD-L pathway like CD55 precursor. Transiently transfected HA-tagged CD48 (HA-CD48) in PIGS-HRD1-DKO cells was stabilized, compared with that in PIGS-KO cells (Fig. 5c). The level of HA-CD48 in PIGS-HRD1-DKO cells was greatly decreased by rescue of HRD1 (Fig. 5c), indicating that CD48 precursor is also under control of ERAD-L pathway.

According to previous reports that replacement of the w-site serine 353 in CD55 with proline abolishes GPI attachment [48], we constructed a CD55(S353P) mutant in which serine was replaced with proline and transiently overexpressed it in PIGS-HRD1-CD55-TKO cells. CD55(S353P) was active in restoring T5 mAb staining (Fig. 5d). Interestingly, the CD55(S353P) mutant was more stable than wild-type CD55 in PIGS-KO cells, in which the ERAD system functioned normally (Fig. 5e). This result raised the possibility that stabilization of CD55 in the ER was the only effect of HRD1-KO in the upregulation of GPI biosynthesis. To validate this hypothesis, we stably overexpressed CD55(S353P) in PIGS-KO cells and isolated two clones, #1 and #2, with different levels of CD55(S353P) (Fig. 5f). Even in the presence of HRD1-dependent ERAD-L pathway, the free GPIs stained by T5 mAb were detected in those cells (Fig. 5g). The T5 mAb staining levels were correlated with the CD55(S353P) protein levels (Fig. 5f-5h). These results indicated that GPI biosynthesis was activated by the GPI attachment signal peptide of CD55 in a dose-dependent manner.

Key residues in GPI attachment signal for GPI biosynthesis

GPI transamidase recognizes and cleaves the GPI attachment signal between ω and ω+1 sites, forming the thioester bond on the catalytic Cys residue to generate an enzyme-substrate intermediate. GPI is then transferred to the newly exposed C-terminus of the protein [47,49]. Although all proteins modified by GPI contain a GPI attachment signal peptide at the C-terminus, the sequences are not conserved. We compared the GPI attachment signal peptide sequences of human CD55, mouse CD55, human CD59 and CD48 and tested their activities. Although human CD55 and mouse CD55 sequences showed some identity, mouse CD55 and human CD59 did not have the ability to restore free GPI expression in PIGS-HRD1-CD55-TKO cells (Fig. 6a). Since the C-terminal GPI attachment signal possesses 5–10 hydrophilic amino acids (spacer sequence) and a 15–20 stretch of hydrophobic amino acids, we truncated the hydrophilic and hydrophobic regions of CD55. Neither truncated construct (T353–361 and T362–381) showed activity (Supplementary Fig. 4a and 4b). We also made chimeras by exchanging hydrophilic and hydrophobic regions of functional CD55 and non-functional CD59, respectively, and overexpressed the constructs in PIGS-HRD1-CD55-TKO cells. Chimeric proteins could not restore T5 mAb staining (Supplementary Fig. 4a and 4b), suggesting that both hydrophilic and hydrophobic regions are important for the activity. We then focused on amino acids among GPI attachment signal sequences and constructed point mutants. Since non-functional CD59 and mouse CD55 had histidine within the hydrophobic region, we introduced histidine into CD55 and CD48 by replacing one of the leucines. The CD55 L371H and CD48 L238H mutants lost activity, even if the mutant proteins were expressed at similar

levels (Fig. 6b-6d). Other CD55 mutants (S353G, L370A, G372A, L373V, and G378Y) maintained the functional activity (Supplementary Fig. 4c and 4d). These findings imply that leucine in the hydrophobic region in the signal peptides played a functionally important role in the regulatory process.

ARV1 is close to and functionally required for CD55 and CD48

With the finding that the GPI attachment signal peptides of CD55 and CD48 directly regulated GPI biosynthesis, we next investigated the underlying mechanism. To identify proteins that might physically interact with them, we used a proximity-tagging system, Turbo-ID. First, we added two functional GPI attachment signal peptides of CD55 and CD48, and two non-functional ones of CD59 and PRNP to the C-terminus of Turbo-ID (Fig. 7a), which were stably expressed in PIGS-HRD1-CD55-TKO cells. TurboID-CD55(C) and TurboID-CD48(C) restored free GPI expression, as expected, whereas TurboID-CD59(C) and TurboID-PRNP(C) had no activity (Fig. 7b-7d). To identify proteins that specifically interacted with CD55, we compared biotinylated proteins by TurboID-CD55(C) and TurboID-CD48(C) with those by TurboID-CD59(C). ARV1 was ranked in the top ten after comparing normalized peptide counts of CD55 with CD59 or CD48 with CD59 (Fig. 7e-7f). To test whether CD55 directly interacted with ARV1, we performed immunoprecipitation experiments by transfecting 3Flag-ARV1 into PIGS-HRD1-CD55-TKO cells stably expressing HA-CD55. We did not detect coprecipitation of ARV1 with CD55 under the tested conditions, suggesting that the interaction was very weak or transient (Supplementary Fig. 5a). The 3Flag-ARV1 levels were similar in the presence or absence of HA-CD55 in PIGS-HRD1-ARV1-TKO cells; therefore, ARV1 and CD55 precursors did not stabilize each other (Supplementary Fig. 5b).

Since both CD55 and ARV1 were required for the upregulation of GPI biosynthesis in HRD1-KO cells, we next asked whether ARV1 was required for the upregulation of GPI biosynthesis by CD55 and CD48. The increased T5 mAb staining level induced by the stable CD55 precursor CD55(S353P) in PIGS-KO cells was decreased to the background level by knocking out ARV1 in CD55(S353P)-expressing PIGS-KO cells (clone #2) and restored by overexpression of 3Flag-ARV1 (Fig. 7g). Overexpression of HA-CD55 or HA-CD48 in PIGS-HRD1-ARV1-TKO cells also could not restore the T5 mAb staining (Supplementary Fig. 5c); therefore, ARV1 was functionally required for CD55 and CD48. These results suggested that CD55/CD48 and ARV1 contributed to the upregulation of GPI biosynthesis in the same pathway.

Finally, we investigated steps in GPI biosynthesis pathway being upregulated by the CD55 precursor. The [2-^{3}H] mannose labeling showed that all spots of GPI intermediates containing mannoses were increased in PIGS-HRD1-DKO cells and their CD55-overexpressing cells (Fig. 3c), indicating that biosynthesis was upregulated by the CD55 precursor, probably at an earlier step before mannose addition. To determine which step was regulated by CD55, [^{3}H]-inositol labeling was performed in PIGW-KO [50], PIGS-KO, PIGS-HRD1-KO, PIGS-HRD1-CD55-TKO, and PIGS-HRD1-ARV1-TKO cells (Fig. 7h). Radioactive inositol was incorporated into PI and then used to generate the first, second, and third GPI intermediates GlcNAc-PI, GlcN-PI, and GlcN-acylPI. After thin-layer chromatography and detection by phosphorimaging, GlcN-PI, which accumulates in PIGW-KO cells, appeared below the abundant PI spots, whereas GlcNAc-PI and GlcN-acylPI did not appear as discrete bands due to overlapping migration with abundant PI and other

inositol-containing components [50]. GlcN-PI was increased in PIGS-HRD1-DKO cells compared to PIGS-KO cells, while knocking out CD55 eliminated GlcN-PI increase, which was rescued by CD55 transfection (Fig. 7h). Knocking out ARV1 similarly prevented the GlcN-PI increase (Fig. 7h), suggesting that both CD55 and ARV1 were required for the upregulation of GPI biosynthesis in a very early step (either the generation of GlcNAc-PI or its conversion into GlcN-PI, or both) (Fig. 8).

Discussion

Although the majority of genes required for GPI precursor biosynthesis, GPI transfer to proteins and GPI remodeling have been identified, understanding the dynamic regulation of GPI biosynthesis is still a challenge. This is in part due to technical obstacles in directly detecting changes in GPI levels. Here, we designed and implemented a free GPI expression system under GPI transamidase- and ERAD-deficient conditions. Detection of free GPI expression provides a new approach for rapidly determining the status of GPI biosynthesis and can be used to understand the regulatory mechanism. In this work, we used the enhancement of free GPI expression in PIGS-HRD1-DKO cells to identify genes that regulate GPI biosynthesis. The screening facilitated the discovery of CD55, which is the substrate of the ERAD-L pathway and upregulates GPI biosynthesis upon accumulation.

Under normal conditions, a GPI attachment signal of precursor protein is recognized and cleaved by GPI transamidase during GPI modification [14]. Most likely, the ratio of GPI and proteins is controlled properly. It is difficult to detect either the accumulation of GPI or precursor proteins in wild-type cells. Normally, misfolded GPI-anchored PrP* (A117V) and Gas1* (G291R) are poor ERAD substrates because of the specific characteristics of GPI anchors [42,43,51]. In stressed mammalian cells, misfolded GPI-anchored PrP* is transported out of the ER quickly via a pathway termed “rapid ER stress-induced export” (RESET) for degradation in the lysosome [51]. However, misfolded transmembrane type Gas1* (Gas1*-TMD) and PrP maintaining its GPI attachment signal peptide that fail to undergo transamidation are mainly degraded by ERAD [42,43]. In this study, we found that knocking out the PIGS and HRD1 genes caused the accumulation of CD55 precursor proteins, which enabled us to reveal the specific role of the GPI attachment signal peptide of CD55 in GPI biosynthesis. It is reasonable to postulate that CD55 acts as a regulator because it is widely expressed in diverse organs and cells [52]. Moreover, we found that the GPI attachment signal peptide of CD48 functioned similarly to that of CD55. The expression of CD48 was restricted to hematopoietic cells, suggesting the existence of other GPI-AP precursors regulating GPI biosynthesis in a tissue-specific manner. Conversely, mouse CD55 could not restore the human CD55 KO phenotype. There are two types of CD55 in mouse cells, the GPI-anchored form and the transmembrane form, which differs from human CD55. We hypothesize that different and diverse GPI-APs are utilized as regulators of GPI biosynthesis among species.

Both our CRISPR–Cas9 genetic screen using PIGS-HRD1-DKO cells and proximity labeling using TurboID-CD55(C) and TurboID-CD48(C) identified ARV1, suggesting that ARV1 is spatially close to and functionally required for CD55. Knocking out ARV1 or CD55 in PIGS-HRD1-DKO cells eliminated the

accumulation of GlcN-PI, resulting in decreased cell surface-free GPI. It is possible that ARV1 and CD55 both work at early stage of GPI biosynthesis. Several papers have reported that Arv1 plays roles in lipid and cholesterol homeostasis, sphingolipid distribution and GPI biosynthesis in the yeast *Saccharomyces cerevisiae* [53,54]. It was proposed that in GPI biosynthesis, Arv1 may deliver early GPI intermediate GlcN-acyPI to the ER lumen as the flippase or contribute to the flip reaction, so the loss of Arv1 leads to deficiencies in GPI-AP biosynthesis in *S. cerevisiae* [55,56]. Furthermore, mutations in human ARV1 cause symptoms similar to inherited GPI deficiencies, indicating that human ARV1 is also involved in GPI biosynthesis [57,58]. A recent study in the African trypanosome *Trypanosoma brucei* showed that an Arv1-like protein (TbArv1) is pulled down by TbGPI3, the mammalian homolog of which is PIGA [59]. Using a combination of RoseTTAFold and AlphaFold, a study to predict protein assemblies with two to five components in *S. cerevisiae* also predicted that ARV1 may interact with Gpi1, the yeast homologue of mammalian PIGQ [60], suggesting that ARV1 may form a complex with GPI N-acetylglucosaminyltransferase (GPI-GnT), the first enzyme in the pathway (Figure S1). In this study, we showed that defects in the HRD1-dependent ERAD-L pathway caused the upregulation of GPI biosynthesis in early steps, but further knockout of CD55 or ARV1 eliminated this effect. CD55 and ARV1 might act together, where CD55 served as the signaling molecule and ARV1 might modulate the proper lipid environments to enhance the activity of GPI-GnT or promote conversion to GlcN-PI; however, we did not find stable interaction between ARV1 and CD55 precursor. It will be interesting to further characterize the relationship between the CD55 precursor and ARV1 in the future.

The expression of free GPIs is sensitive to ARV1 or CD55 KO, indicating that ARV1 is critical for the upregulation of GPI biosynthesis, particularly under conditions where GPI-AP precursor proteins, including CD55, accumulate. However, in HEK293 wild-type cells, knockout of ARV1 or CD55 did not change the expression of GPI-APs, suggesting that they play roles only in GPI biosynthesis under stressed conditions. Since the expression of known PIG genes was not changed in the presence or absence of CD55 and overexpression of PIG genes did not restore free GPI expression in PIGS-HRD1-CD55-TKO cells, the regulation was neither at the transcriptional nor the translational level of GPI biosynthetic genes. Thus, the upregulation of GPI biosynthesis by CD55 precursors is a rather quick and short-lived quantity control system for GPI-APs once the downstream GPI transamidation step fails in wild-type cells. It is possible that CD55 and ARV1 are involved in this regulatory system to balance the biosynthesis of free GPIs and the generation of GPI-APs in the ER.

Methods

Cell culture, transfection, and stable cell line generation

HEK293 (ATCC CRL-1573) cells and all derivative cells were cultured in Dulbecco's modified Eagle's medium (DMEM) with high glucose, glutamine (01-052-1ACS, Biological Industries) and 10% fetal bovine serum (FBS) (04-001-1ACS, Biological Industries) at 37 °C in a humidified 5% CO_2 atmosphere. PIGK-KO, GPAA1-KO, PIGT-KO, PIGS-KO, PIGU-KO, PIGS-HRD1-DKO, PIGS-UBE2G2-DKO, PIGS-UBE2J1-DKO, PIGS-

GP78-DKO, and SLC35A2-PIGT-DKO cells were previously constructed [26]. The PIGK-HRD1-DKO, PIGT-HRD1-DKO, PIGU-HRD1-DKO, GPAA1-HRD1-DKO, SLC35A2-PIGT-HRD1-TKO, PIGS-HRD1-SRD5A3-TKO, PIGS-HRD1-ARV1-TKO, PIGS-HRD1-CD55-TKO, PIGS-HRD1-SPPL3-TKO, and PIGS-HRD1-CLPTM1L-TKO cells used in this study were established by the CRISPR/Cas9 system with two different gRNAs, as listed in Supplementary Data 1. For stable expression, PLAT-GP packaging cells were seeded and cultured to 90% confluence and transfected with the pLIB2-BSD plasmid bearing the cDNA of interest using PEI-Max. Viral medium was added to the cells, and these cells were cultured at 32 °C for 12 h. The medium was changed after 24 h and cultured at 37 °C. Three days after infection, the cells were incubated in the medium with 10 μg/mL blasticidin (InvivoGen) for 14 days.

Antibodies and reagents

The mouse monoclonal anti-*Toxoplasma gondii* free GPI (clone T5 4E10) (1:100 for flow cytometric analysis or FACS) antibody (T5 mAb) was a generous gift from Dr. Jean François Dubremetz (Montpellier University, France) [20]. T5 mAb (50267) is now available from BEI Resources, NIAID, NIH. Mouse monoclonal anti-CD55 (clone IA10) (1:100 for flow cytometric analysis or FACS; 1:500 for western blot or WB)[61], anti-CD59 (clone 5H8) (1:100 for FACS)[62], anti-Flag (F3165, Sigma) (1:4000 for WB), anti-calnexin (M178-3; MBL) (1:4000 for WB), anti-CD147 (sc-71038, Santa Cruz Biotechnology) (1:1000 for WB), anti-GAPDH (60004-1-Ig, Proteintech) (1:4000 for WB), rabbit monoclonal anti-HA (3724, Cell Signaling Technology) (1:4000 for WB), and polyclonal anti-GFP (50430-2-AP, Proteintech) (1:4000 for WB) were used as primary antibodies. $F(ab')_2$-goat anti-mouse IgG (H+L) PE (12-4010-82; Thermo Fisher Scientific) (1:200 for FACS), Alexa Fluor 647-conjugated goat against mouse IgM (ab150123, Abcam) (1:400 for FACS), goat anti-mouse IgG (H+L) HRP (HS201, TransGen Biotech) (1:5000 for WB), goat anti-rabbit IgG (H+L) HRP (HS101, TransGen Biotech) (1:5000 for WB), Alexa Fluor 488-conjugated goat anti-mouse IgG (A-11008, Thermo Fisher Scientific) (1:500 for IF), and Alexa Fluor 555-conjugated goat anti-rabbit IgG (A-21424, Thermo Fisher Scientific) (1:500 for IF) were used as secondary antibodies. PNGase F (P0704, New England Biolabs) and Endo Hf (P0703, New England Biolabs) were used for cleavage of N-glycans. Biotin (V900418, Sigma) was used for proximity labeling.

CRISPR–Cas9 screening and FACS

For a large-pooled screen, viral production and functional titration were conducted in the same manner as described previously [26]. Pooled human GeCKOv2 plasmids (lentiCRISPRv2) were cotransfected with the lentiviral packaging plasmids pLP1, pLP2, and pLP/VSVG (Thermo Fisher) into Lenti-X 293T cells (Clontech). Twelve hours later, the medium was changed to 10 mL prewarmed DMEM supplemented with 10% FBS. The viral media was collected 24 h, 48 h, and 72 h after transfection and filtered through a

membrane (Mllex 0.45 μm, PVDF, 33 mm). Finally, 30 mL viral media in total was combined and stored at 4 °C for functional titration and pooled screening as quickly as possible.

PIGS-HRD1-DKO cells were plated in 8 × 15 cm dishes (3.5 ×10^6 cells per dish). Approximately 8 × 10^7 cells (1 ×10^7 cells per dish) were transduced with viral supernatant after 36 h of seeding. Cells were selected with 0.5 μg/mL puromycin until the infected cells were expanded to 2.4 × 10^8 to maintain the complexity of the gRNA library. Cells were combined and split 1:4, and a minimum of 6 × 10^7 cells were plated for culture. At 2 weeks posttransduction, a pellet of 5 × 10^7 cells without sorting was stored at -80 °C. For cell sorting, approximately 1 × 10^8 cells were harvested and incubated with T5 mAb, followed by staining with anti-mouse IgM. After washing with PBS, the cells were resuspended in Hanks' Balanced Salt Solution (H6648, Sigma-Aldrich), and T5 mAb staining-negative cells were sorted by FACSAria (BD). We prepared 2 × 10^7 cells for the second sorting. After sorting, the cells were maintained in DMEM supplemented with 0.25 μg/mL puromycin. Pellets of 2 × 10^7 sort2 cells were stored at -80 °C until use. For analysis, cells were cultured in 6-well plates one day before analysis. The cells were harvested and washed once with PBS and then stained with CD59 or T5 mAb in FACS solution (PBS containing 1% BSA and 0.1% NaN_3) on ice for 25 min. They were then washed twice in FACS buffer, followed by staining with Alexa Fluor 647-conjugated goat anti-mouse IgM or PE-conjugated goat anti-mouse IgG. After two washes with FACS buffer, the cells were analyzed using a BD FACSCanto II.

Genomic DNA sequencing and analysis

Approximately 5 × 10^7 unsorted and 2 × 10^7 twice-sorted PIGS-HRD1-DKO cells were extracted for genomic DNA using a Wizard Genomic DNA Purification Kit (Promega). The gRNAs were amplified from genomic DNA of unsorted and twice-sorted cells. PCR (25 cycles) was performed to amplify the gRNAs using KOD FX Neo Polymerase (TOYOBO LIFE SCIENCE), making up a total of 65 tubes for unsorted cells and 12 tubes for twice-sorted cells (oligos for amplification of gRNAs are shown in Supplementary Data 1). All PCR products were combined and mixed and applied to a 2% agarose gel for purification. The PCR products were concentrated, mixed 9:1, and analyzed by paired-end sequencing with a NovaSeq 6000 system (Illumina). Deep sequencing raw data were processed for gRNA counting using Python scripts. The high-throughput sequencing reads were demultiplexed using the 5-bp adapter by cutadapt version v1.18 [63]. By using MAGeCK workflow version 0.5.6, the adapters of the demultiplexed reads were trimmed to obtain 20-bp gRNA sequences, and the sgRNA sequences were mapped to the sequences of the Human GeCKO v2 sgRNA library to determine the total number of gRNA counts. The robust rank aggregation (RRA) values and p values were determined using the MAGeCK algorithm [64].

Plasmids

All primers used in this study are listed in Table S1. To knock out target genes with the CRISPR–Cas9 system, single-guide RNAs (sgRNAs) were designed with the E-CRISP website (http://www.e-crisp.org/E-CRISP/), and the targeting DNA fragments were ligated into the BbsI-digested vector pX330-EGFP. To construct pME-HRD1-3HA and pME-SPPL3-3HA, HRD1 and SPPL3 were amplified from a human cDNA library, digested with XhoI and MulI, and were cloned into the same site of pME-B3GALT4-3HA. The HRD1-3HA fragment from pME-HRD1-3HA was digested and ligated to pLIB2-BSD through EcoRI and NotI. SRD5A3 and CLPTM1L fragments were digested with EcoRI and NotI, and pLIB2-BSD-SRD5A3 and pLIB2-BSD-CLPTM1L were constructed. The fragment of ARV1 was digested with SalI and NotI and ligated into pME-3Flag to construct pME-3Flag-ARV1. Human CD55, CD48, CD59, PRNP, and mouse CD55 (mCD55) were amplified, digested and ligated into pME-puro-ssHA-GPI, which contains a CD59 signal sequence, one HA tag and a GPI attachment signal sequence of CD55, through XhoI and NotI to generate pME-puro-ssHA-CD55, pME-puro-ssHA-CD48, pME-puro-ssHA-CD59, pME-puro-ssHA-PRNP, and pME-puro -ssHA-mCD55. GPI attachment signals of CD55 and CD48 were amplified from pME-puro-ssHA-CD55 and pME-puro-ssHA-CD48 and cloned into pME-ssGFP to generate pME-ssGFP-CD55(C) and pME-ssGFP-CD48(C). The ssGFP-CD55(C) fragment was cut with EcoRI and NotI and ligated into pLIB2-BSD to generate pLIB2-BSD-ssGFP-CD55(C). pME-ssHA-CD55 was used as a template and mutagenized with different primers to construct truncated CD55. Plasmids harboring mutant CD55, CD48 or CD55(C) were constructed by site-direct mutagenesis based on pME-puro-ssHA-CD55, pME-puro-ssHA-CD48, pME-puro-ssHA-mCD55 and pLIB2-BSD-ssGFP-CD55(C). 3HA-TurboID was amplified from 3xHA-TurboID-NLS_pCDNA (3107171, Addgene) and cloned into pME-ssCD59-EGFP to generate pME-ssCD59-3HA-TurboID. The GPI attachment signals of CD55, CD48, CD59, and PRNP were amplified and ligated into pME-ssCD59-3HA-TurboID-CD55(C), pME-ssCD59-3HA-TurboID-CD48(C), pME-ssCD59-3HA-TurboID-CD59(C), and pME-ssCD59-3HA-TurboID-PRNP(C), followed by digestion with EcoRI and NotI and cloned into pLIB2-BSD.

Generation of knockout cell lines

To knock out SRD5A3, ARV1, CD55, SPPL3, and CLPTM1L, cells were transfected with one or two different pX330-EGFPs containing the target sgRNA. Lipofectamine 2000 (11668019, Thermo Fisher Scientific) was used for transfection. Three days after transfection, the GFP-positive cells were sorted with a cell sorter S3e (Bio–Rad). The sorted cells were cultured for one week or more and then diluted to select clonal KO cells. Clonal cells were determined by rescue experiments and western blotting analysis. Knockout of HRD1 in PIGK-KO, GPAA1-KO, PIGT-KO, PIGU-KO or CD59, PRNP, GPC4, CD109, LY6E in PIGS-HRD1-DKO cells was carried out within the bulk cells. After transient transfection of sgRNA constructs as described above, the bulk cells were sorted and cultured for 10 days, followed by flow cytometry analysis.

SDS–PAGE and Western-blotting

Western blotting was performed to confirm the expression of recombinant proteins. Cells (~10^6 cells/well) were lysed with 60 μL of RIPA lysis buffer (50 mM Tris pH 8, 150 mM NaCl, 0.1% SDS, 0.5% sodium deoxycholate, 1% Triton X-100, 1 mM phenylmethylsulfonyl fluoride (HY-B0496, MedChemExpress), protease inhibitor cocktail (HY-K0010, MedChemExpress)) on ice for 30 min. After incubation, the sample was centrifuged at 21,600 x g for 10 min at 4 °C to remove the insoluble fraction. The supernatant was mixed with SDS–PAGE loading buffer and boiled at 95 °C for 5 min or kept at 4 °C overnight (for multitransmembrane proteins). The proteins were separated by SDS–PAGE and transferred onto PVDF membranes, and the membranes were blocked at room temperature (RT) in Tris-buffered saline containing 0.1% Tween-20 (TBS-T) and 5% nonfat milk for 1 h, followed by incubation with primary antibodies at RT for 1 h. After washing three times with TBS-T buffer, the membranes were then incubated with horseradish peroxidase-labeled secondary antibodies for 1 h at RT. After washing with TBS-T, the membrane was visualized with ECL Prime western blotting Detection Reagent (GE Health care).

Immunofluorescence

To detect the subcellular localization of HA-tagged CD55, PIGS-HRD1-CD55-TKO cells stably expressing HA-CD55 were seeded on glass coverslips pretreated with 1% gelatin and cultured for another 2 days. Cells were washed with PBS, fixed in 4% paraformaldehyde, washed with PBS, and incubated with 40 mM ammonium chloride. Then, the cells were incubated at RT in blocking buffer A (PBS containing 5% FBS) for 1 h. Mouse anti-calnexin (M178–3; MBL) and rabbit monoclonal anti-HA (3724, Cell Signaling Technology) were used as the primary antibodies diluted in blocking buffer for 1 h. Cells were gently washed with PBS twice. Alexa Fluor 555-conjugated goat anti-rabbit IgG (A-21424, Thermo Fisher Scientific) and Alexa Fluor 488-conjugated goat anti-mouse IgG (A-11008, Thermo Fisher Scientific) were used as the secondary antibodies and diluted in blocking buffer for 1 h. The cells were gently washed with PBS twice. Finally, the coverslips were mounted onto slides using a mounting solution containing DAPI for 5 min and visualized under a confocal microscope (C2si; Nikon).

RNA sequencing

RNA sequencing and analysis were conducted as previously described [65]. Total RNA was extracted from whole cells with the mirVana miRNA Isolation Kit (Thermo Fisher Scientific) according to the manufacturer's protocol. RNA quality and integrity were evaluated with an Agilent 2100 Bioanalyzer (Agilent Technologies, Santa Clara, California, USA). Samples with an RNA integrity number (RIN) ≥ 7 were considered to be of high quality and were processed further and subjected to subsequent analysis. Total RNA-seq libraries were generated using 4 μg of total RNA, which was analyzed using the TruSeq Stranded mRNA LTSample Prep Kit (Illumina, San Diego, CA, USA). These libraries were then sequenced using the Illumina sequencing platform (HiSeqTM 2500 or Illumina HiSeq X Ten), and 125-bp/150-bp

paired-end reads were generated. Transcriptome sequencing was conducted by OE Biotech Co., Ltd. (Shanghai, China), and clean reads were provided. The clean reads were mapped to the hg38 reference genome using hisat2 (version 2.1.0). The output BAM files were converted to SAM files using SAMtools 1.9. The final TPM values were obtained using Stringtie 1.3.5.

In vivo metabolic labeling of GPI intermediates

The process of labeling experiments followed a previous protocol [26]. For mannose labeling, approximately 2 × 10^6 PIGS-KO, PIGS-HRD1-DKO, and PIGS-HRD1-CD55-TKO cells, and PIGS-HRD1-CD55-TKO cells stably expressing HA-CD55 were precultured in normal medium overnight, washed with wash medium (glucose-free DMEM buffered with 20 mM HEPES, pH 7.4) and incubated for 1 h at 37 °C in 1 mL of reaction medium (wash medium supplemented with 10% dialyzed FBS (Gibco), 10 μg/mL tunicamycin (Wako), and 100 μg/mL glucose). The [2-^{3}H] mannose (American Radiolabeled Chemicals) was added to 25 Ci/ml, and the cells were incubated for 1 h at 37 °C in 5% CO_2. The cells were pelleted and washed with 1 ml of cold PBS. Radiolabeled GPIs were extracted with 1-butanol, separated by HPTLC (Merck), and visualized using an FLA 7000 analyzer (Fujifilm).

To detect GlcN-PI or GlcN-(acyl)-PI after inositol-labeling, PIGW-KO, PIGS-KO, PIGS-HRD1-DKO, PIGS-HRD1-ARV1-TKO, PIGS-HRD1-CD55-TKO and HA-CD55 rescued cells were washed with inositol-free DMEM and then incubated in 1 mL of reaction medium B (inositol-free DMEM buffered with 20 mM HEPES, pH 7.4) supplemented with 10% dialyzed FBS in the presence of 10 μCi of myo-[2-^{3}H] inositol (PerkinElmer) for 24 h. After metabolic labeling, the cells were washed twice with 1 mL of cold PBS and pelleted by centrifugation. Lipids and radiolabeled GPIs were extracted with 1-butanol partitioning, separated by HPTLC (Merck), and visualized using an FLA 7000 analyzer.

Proximity labeling assay

For biotin labeling, the major process followed the protocol described by Alice Ting's group [66]. PIGS-HRD1-CD55-TKO cells stably expressing TurboID-CD55(C), TurboID-CD48(C) or TurboID-CD59(C) were seeded in 5 × 15 cm dishes and cultured in normal medium to reach 100% confluence. From a 100 mM biotin stock in dimethyl sulfoxide (DMSO), we diluted biotin directly into serum-containing cell culture medium to the desired final concentration of 500 μM biotin. Labeling was stopped after 2 h by transferring the cells to ice and washing them five times with ice-cold PBS. The cells were harvested and washed with PBS and lysed in 5 mL RIPA lysis buffer by gentle pipetting and rotating for 1 h at 4 °C. Lysates were clarified by centrifugation at 21,600 x g for 10 min at 4 °C, followed by collection of the supernatant in a new tube. To enrich biotinylated material from samples, 250 μL StrepTactin Sepharose (28-9355-99, GE) was added to the supernatant and rotated for 1 h at 4 °C. The Sepharose was washed twice with 1 mL of RIPA lysis buffer, once with 1 mL of 1 M KCl, once with 1 mL of 0.1 M Na_2CO_3, once

with 1 mL of 2 M urea in 10 mM Tris-HCl (pH 8.0), and twice with 1 mL RIPA lysis buffer. The beads were then resuspended in 0.5 mL fresh RIPA lysis buffer, transferred to a new Eppendorf tube, and stored at -80 °C for further processing and preparation for LC-MS/MS analysis.

Mass spectrometry analysis

To prepare samples for mass spectrometry analysis, proteins bound to streptavidin beads were washed twice with 200 µL of 50 mM Tris HCl buffer (pH 7.5) followed by two washes with 0.8 M urea/40 mM NH_4HCO_3 buffer. The beads were incubated with 200 µL of 0.8 M urea/40 mM NH_4HCO_3 containing 10 mM DTT incubated for 1 h at 37 °C with shaking, followed by alkylation with 10 mM iodoacetamide for 45 min in the dark at 37 °C with shaking. Then, 4 µg trypsin was added to the sample and another 4 µg trypsin was added to the mixture overnight at 37 °C with shaking. After overnight digestion, the samples were acidified (to pH < 3) by addition of formic acid (FA). The samples were desalted on C18 StageTips and evaporated to dryness in a vacuum concentrator.

For TMT labeling, desalted peptides were labeled with TMT (6-plex) reagents according to the manufacturer's protocol. Peptides were reconstituted in 100 µL of 50 mM HEPES. Each 0.8 mg vial of TMT reagent was reconstituted in 41 µL of anhydrous acetonitrile (MeCN) and added to the corresponding peptide sample for 1 h at RT. TMT labeling reactions were quenched with 8 µL of 5% hydroxylamine at RT for 15 min with shaking, evaporated to dryness in a vacuum concentrator, and desalted on C18 StageTips. For each TMT 6-plex cassette, 50% of the sample was fractionated by basic pH reverse phase using StageTips, while the other 50% of each sample was reserved for LC-MS analysis using a single-shot, long gradient. One StageTip was prepared per sample using 2 plugs of styrene divinylbenzene (SDB) (3M) material. The StageTips were conditioned two times with 50 µL of 100% methanol, followed by 50 µL of 50% MeCN/0.1% FA, and two times with 75 µL of 0.1% FA. The sample, resuspended in 100 µL of 0.1% FA, was loaded onto the stage tips and washed with 100 µL of 0.1% FA. Subsequently, the sample was washed with 60 µL of 20 mM NH_4HCO_2/2% MeCN, and this wash was saved and added to fraction 1. The sample was then eluted from StageTip using the following concentrations of MeCN in 20 mM NH_4HCO_2: 10%, 15%, 20%, 25%, 30%, 40%, and 50%. For a total of 6 fractions, the 10 and 40% (fractions 2 and 7) elutions were combined, as well as the 15 and 50% elutions (fractions 3 and 8). The six fractions were dried by vacuum centrifugation.

The dried peptides were resuspended in 15 µL of 2% MeCN and 0.1% FA solution and then analyzed using an EASY-nLC 1200 system (Thermo Scientific, San Jose, CA) coupled with a high-resolution Orbitrap Fusion Lumos spectrometer (Thermo Scientific, San Jose, CA). Each injection volume was 3 µL. The samples were first separated on an EASY-nLC 1200 system with an RSLC C18 column (1.9 µm ×100 µm ×20 cm) packed in house.

Statistical analysis

Statistical analysis was determined using the Student's t-test (GraphPad Prism 8.0 software; GraphPad software Inc., La Jolla, CA) to evaluate comparisons between three individual experiments, and p values < 0.05 were considered statistically significant.

Data availability

The source data underlying Figs. 1C and F, Fig. 2E, Fig. 4C, Fig. 5H, Fig. 6C and Fig. 7C, and Supplementary Figs. 1D are provided as a Source Data file. Uncropped western blot images are available in Supplementary Fig. S6. RNA Sequencing data are available in Supplementary Data 2 and from the GEO database under accession number GSE184822 (RNA sequencing of PIGS-KO, PIGS-HRD1-DKO, PIGS-HRD1-CD55-TKO and PIGS-HRD1-CD55-TKO+HA-CD55 cells). The mass spectrometry proteomics data have been deposited to the ProteomeXchange Consortium via the PRIDE76 partner repository with the dataset identifier PXD028707 (project name: Determination of proteins labeling by Turbo-ID in PIGS-HRD1-CD55-TKO cells). All other data that support the findings of this study are available from the corresponding author upon reasonable request.

References

1. Schwarz, D. S. & Blower, M. D. The endoplasmic reticulum: structure, function and response to cellular signaling. *Cell Mol Life Sci* **73**, 79–94, doi:10.1007/s00018-015-2052-6 (2016).
2. Braakman, I. & Hebert, D. N. Protein folding in the endoplasmic reticulum. *Cold Spring Harb Perspect Biol* **5**, a013201, doi:10.1101/cshperspect.a013201 (2013).
3. Clapham, D. E. Calcium signaling. *Cell* **131**, 1047–1058, doi:10.1016/j.cell.2007.11.028 (2007).
4. Sicari, D., Igbaria, A. & Chevet, E. Control of Protein Homeostasis in the Early Secretory Pathway: Current Status and Challenges. *Cells* **8**, doi:10.3390/cells8111347 (2019).
5. Helenius, A. & Aebi, M. Roles of N-linked glycans in the endoplasmic reticulum. *Annu Rev Biochem* **73**, 1019–1049, doi:10.1146/annurev.biochem.73.011303.073752 (2004).
6. Liu, Y. S. & Fujita, M. Mammalian GPI-anchor modifications and the enzymes involved. *Biochem Soc Trans* **48**, 1129–1138, doi:10.1042/BST20191142 (2020).
7. Kinoshita, T. Biosynthesis and biology of mammalian GPI-anchored proteins. *Open Biol* **10**, 190290, doi:10.1098/rsob.190290 (2020).
8. Nozaki, M. *et al.* Developmental abnormalities of glycosylphosphatidylinositol-anchor-deficient embryos revealed by Cre/loxP system. *Lab Invest* **79**, 293–299 (1999).
9. Um, J. W. & Ko, J. Neural Glycosylphosphatidylinositol-Anchored Proteins in Synaptic Specification. *Trends Cell Biol* **27**, 931–945, doi:10.1016/j.tcb.2017.06.007 (2017).

10. Wang, Y. *et al.* Significance of glycosylphosphatidylinositol-anchored protein enrichment in lipid rafts for the control of autoimmunity. *J Biol Chem* **288**, 25490–25499, doi:10.1074/jbc.M113.492611 (2013).
11. Watanabe, H., Takeda, R., Hirota, K. & Kondoh, G. Lipid raft dynamics linked to sperm competency for fertilization in mice. *Genes Cells* **22**, 493–500, doi:10.1111/gtc.12491 (2017).
12. Orlean, P. & Menon, A. K. Thematic review series: lipid posttranslational modifications. GPI anchoring of protein in yeast and mammalian cells, or: how we learned to stop worrying and love glycophospholipids. *J Lipid Res* **48**, 993–1011, doi:10.1194/jlr.R700002-JLR200 (2007).
13. Pittet, M. & Conzelmann, A. Biosynthesis and function of GPI proteins in the yeast Saccharomyces cerevisiae. *Biochim Biophys Acta* **1771**, 405–420, doi:10.1016/j.bbalip.2006.05.015 (2007).
14. Liu, S. S. *et al.* A knockout cell library of GPI biosynthetic genes for functional studies of GPI-anchored proteins. *Commun Biol* **4**, 777, doi:10.1038/s42003-021-02337-1 (2021).
15. Kinoshita, T. & Fujita, M. Biosynthesis of GPI-anchored proteins: special emphasis on GPI lipid remodeling. *J Lipid Res* **57**, 6–24, doi:10.1194/jlr.R063313 (2016).
16. Fujita, M. *et al.* GPI glycan remodeling by PGAP5 regulates transport of GPI-anchored proteins from the ER to the Golgi. *Cell* **139**, 352–365, doi:10.1016/j.cell.2009.08.040 (2009).
17. Hirata, T. *et al.* Identification of a Golgi GPI-N-acetylgalactosamine transferase with tandem transmembrane regions in the catalytic domain. *Nat Commun* **9**, 405, doi:10.1038/s41467-017-02799-0 (2018).
18. Kobayashi, A. *et al.* alpha2,3 linkage of sialic acid to a GPI anchor and an unpredicted GPI attachment site in human prion protein. *J Biol Chem* **295**, 7789–7798, doi:10.1074/jbc.RA120.013444 (2020).
19. Sharma, S. D., Mullenax, J., Araujo, F. G., Erlich, H. A. & Remington, J. S. Western Blot analysis of the antigens of Toxoplasma gondii recognized by human IgM and IgG antibodies. *J Immunol* **131**, 977–983 (1983).
20. Striepen, B. *et al.* Molecular structure of the "low molecular weight antigen" of Toxoplasma gondii: a glucose alpha 1-4 N-acetylgalactosamine makes free glycosyl-phosphatidylinositols highly immunogenic. *J Mol Biol* **266**, 797–813, doi:10.1006/jmbi.1996.0806 (1997).
21. Tomavo, S. *et al.* Immunolocalization and characterization of the low molecular weight antigen (4-5 kDa) of Toxoplasma gondii that elicits an early IgM response upon primary infection. *Parasitology* **108** (**Pt 2**), 139–145, doi:10.1017/s0031182000068220 (1994).
22. Wang, Y. *et al.* Free, unlinked glycosylphosphatidylinositols on mammalian cell surfaces revisited. *J Biol Chem* **294**, 5038–5049, doi:10.1074/jbc.RA119.007472 (2019).
23. Singh, N., Liang, L. N., Tykocinski, M. L. & Tartakoff, A. M. A novel class of cell surface glycolipids of mammalian cells. Free glycosyl phosphatidylinositols. *J Biol Chem* **271**, 12879–12884, doi:10.1074/jbc.271.22.12879 (1996).
24. Baumann, N. A., Vidugiriene, J., Machamer, C. E. & Menon, A. K. Cell surface display and intracellular trafficking of free glycosylphosphatidylinositols in mammalian cells. *J Biol Chem* **275**, 7378–7389,

doi:10.1074/jbc.275.10.7378 (2000).

25. Duval, R. *et al.* Inherited glycosylphosphatidylinositol defects cause the rare Emm-negative blood phenotype and developmental disorders. *Blood* **137**, 3660–3669, doi:10.1182/blood.2020009810 (2021).
26. Wang, Y. *et al.* Cross-talks of glycosylphosphatidylinositol biosynthesis with glycosphingolipid biosynthesis and ER-associated degradation. *Nat Commun* **11**, 860, doi:10.1038/s41467-020-14678-2 (2020).
27. Sun, Z. & Brodsky, J. L. Protein quality control in the secretory pathway. *J Cell Biol* **218**, 3171–3187, doi:10.1083/jcb.201906047 (2019).
28. Neal, S. *et al.* The Dfm1 Derlin Is Required for ERAD Retrotranslocation of Integral Membrane Proteins. *Mol Cell* **69**, 306-320 e304, doi:10.1016/j.molcel.2017.12.012 (2018).
29. Baldridge, R. D. & Rapoport, T. A. Autoubiquitination of the Hrd1 Ligase Triggers Protein Retrotranslocation in ERAD. *Cell* **166**, 394–407, doi:10.1016/j.cell.2016.05.048 (2016).
30. Lemberg, M. K. & Strisovsky, K. Maintenance of organellar protein homeostasis by ER-associated degradation and related mechanisms. *Mol Cell* **81**, 2507–2519, doi:10.1016/j.molcel.2021.05.004 (2021).
31. Wu, X. *et al.* Structural basis of ER-associated protein degradation mediated by the Hrd1 ubiquitin ligase complex. *Science* **368**, doi:10.1126/science.aaz2449 (2020).
32. Habeck, G., Ebner, F. A., Shimada-Kreft, H. & Kreft, S. G. The yeast ERAD-C ubiquitin ligase Doa10 recognizes an intramembrane degron. *J Cell Biol* **209**, 261–273, doi:10.1083/jcb.201408088 (2015).
33. Shi, J. *et al.* A technique for delineating the unfolding requirements for substrate entry into retrotranslocons during endoplasmic reticulum-associated degradation. *J Biol Chem* **294**, 20084–20096, doi:10.1074/jbc.RA119.010019 (2019).
34. Leto, D. E. *et al.* Genome-wide CRISPR Analysis Identifies Substrate-Specific Conjugation Modules in ER-Associated Degradation. *Mol Cell* **73**, 377-389 e311, doi:10.1016/j.molcel.2018.11.015 (2019).
35. Schoebel, S. *et al.* Cryo-EM structure of the protein-conducting ERAD channel Hrd1 in complex with Hrd3. *Nature* **548**, 352–355, doi:10.1038/nature23314 (2017).
36. Peterson, B. G., Glaser, M. L., Rapoport, T. A. & Baldridge, R. D. Cycles of autoubiquitination and deubiquitination regulate the ERAD ubiquitin ligase Hrd1. *Elife* **8**, doi:10.7554/eLife.50903 (2019).
37. Vasic, V. *et al.* Hrd1 forms the retrotranslocation pore regulated by auto-ubiquitination and binding of misfolded proteins. *Nat Cell Biol* **22**, 274–281, doi:10.1038/s41556-020-0473-4 (2020).
38. Sanjana, N. E., Shalem, O. & Zhang, F. Improved vectors and genome-wide libraries for CRISPR screening. *Nat Methods* **11**, 783–784, doi:10.1038/nmeth.3047 (2014).
39. Wang, Y. *et al.* CLPTM1L is a lipid scramblase involved in glycosylphosphatidylinositol biosynthesis. *bioRxiv* (2021).
40. Davis, E. M. *et al.* Comparative Haploid Genetic Screens Reveal Divergent Pathways in the Biogenesis and Trafficking of Glycophosphatidylinositol-Anchored Proteins. *Cell Rep* **11**, 1727–1736,

doi:10.1016/j.celrep.2015.05.026 (2015).

41. Kawaguchi, K., Yamamoto-Hino, M. & Goto, S. SPPL3-dependent downregulation of the synthesis of (neo)lacto-series glycosphingolipid is required for the staining of cell surface CD59. *Biochem Biophys Res Commun* **571**, 81–87, doi:10.1016/j.bbrc.2021.06.093 (2021).
42. Ashok, A. & Hegde, R. S. Retrotranslocation of prion proteins from the endoplasmic reticulum by preventing GPI signal transamidation. *Mol Biol Cell* **19**, 3463–3476, doi:10.1091/mbc.E08-01-0087 (2008).
43. Sikorska, N. *et al.* Limited ER quality control for GPI-anchored proteins. *J Cell Biol* **213**, 693–704, doi:10.1083/jcb.201602010 (2016).
44. He, Y. *et al.* Structure of decay-accelerating factor bound to echovirus 7: a virus-receptor complex. *Proc Natl Acad Sci U S A* **99**, 10325–10329, doi:10.1073/pnas.152161599 (2002).
45. Coyne, K. E. *et al.* Mapping of epitopes, glycosylation sites, and complement regulatory domains in human decay accelerating factor. *J Immunol* **149**, 2906–2913 (1992).
46. White, J. *et al.* Biological activity, membrane-targeting modification, and crystallization of soluble human decay accelerating factor expressed in E. coli. *Protein Sci* **13**, 2406–2415, doi:10.1110/ps.03455604 (2004).
47. Yang, J. *et al.* Human SND2 mediates ER targeting of GPI-anchored proteins with low hydrophobic GPI attachment signals. *Febs Lett* **595**, 1542–1558, doi:10.1002/1873-3468.14083 (2021).
48. Moran, P., Raab, H., Kohr, W. J. & Caras, I. W. Glycophospholipid Membrane Anchor Attachment - Molecular Analysis of the Cleavage Attachment Site. *Journal of Biological Chemistry* **266**, 1250–1257 (1991).
49. Eisenhaber, B., Eisenhaber, S., Kwang, T. Y., Gruber, G. & Eisenhaber, F. Transamidase subunit GAA1/GPAA1 is a M28 family metallo-peptide-synthetase that catalyzes the peptide bond formation between the substrate protein's omega-site and the GPI lipid anchor's phosphoethanolamine. *Cell Cycle* **13**, 1912–1917, doi:DOI 10.4161/cc.28761 (2014).
50. Murakami, Y. *et al.* PIG-W is critical for inositol acylation but not for flipping of glycosylphosphatidylinositol-anchor. *Mol Biol Cell* **14**, 4285–4295, doi:10.1091/mbc.e03-03-0193 (2003).
51. Satpute-Krishnan, P. *et al.* ER stress-induced clearance of misfolded GPI-anchored proteins via the secretory pathway. *Cell* **158**, 522–533, doi:10.1016/j.cell.2014.06.026 (2014).
52. Karlsson, M. *et al.* A single-cell type transcriptomics map of human tissues. *Sci Adv* **7**, doi:10.1126/sciadv.abh2169 (2021).
53. Swain, E. *et al.* Yeast cells lacking the ARV1 gene harbor defects in sphingolipid metabolism. Complementation by human ARV1. *J Biol Chem* **277**, 36152–36160, doi:10.1074/jbc.M206624200 (2002).
54. Georgiev, A. G. *et al.* Arv1 Regulates PM and ER Membrane Structure and Homeostasis But is Dispensable for Intracellular Sterol Transport. *Traffic* **14**, 912–921, doi:10.1111/tra.12082 (2013).

55. Kajiwara, K. *et al.* Yeast ARV1 is required for efficient delivery of an early GPI intermediate to the first mannosyltransferase during GPI assembly and controls lipid flow from the endoplasmic reticulum. *Mol Biol Cell* **19**, 2069–2082, doi:10.1091/mbc.E07-08-0740 (2008).
56. Okai, H. *et al.* Cold-sensitive phenotypes of a yeast null mutant of ARV1 support its role as a GPI flippase. *Febs Lett* **594**, 2431–2439, doi:10.1002/1873-3468.13843 (2020).
57. Ikeda, A. *et al.* Complementation analysis reveals a potential role of human ARV1 in GPI anchor biosynthesis. *Yeast* **33**, 37–42, doi:10.1002/yea.3138 (2016).
58. Salian, S. *et al.* Epileptic encephalopathy caused by ARV1 deficiency: Refinement of the genotype-phenotype spectrum and functional impact on GPI-anchored proteins. *Clin Genet*, doi:10.1111/cge.14033 (2021).
59. Ji, Z., Tinti, M. & Ferguson, M. A. J. Proteomic identification of the UDP-GlcNAc: PI alpha1-6 GlcNAc-transferase subunits of the glycosylphosphatidylinositol biosynthetic pathway of Trypanosoma brucei. *PLoS One* **16**, e0244699, doi:10.1371/journal.pone.0244699 (2021).
60. Humphreys, I. R. *et al.* Structures of core eukaryotic protein complexes. *bioRxiv*, 2021.2009.2030.462231, doi:10.1101/2021.09.30.462231 (2021).
61. Kinoshita, T., Medof, M. E., Silber, R. & Nussenzweig, V. Distribution of decay-accelerating factor in the peripheral blood of normal individuals and patients with paroxysmal nocturnal hemoglobinuria. *J Exp Med* **162**, 75–92, doi:10.1084/jem.162.1.75 (1985).
62. Ashida, H. *et al.* Mammalian PIG-X and yeast Pbn1p are the essential components of glycosylphosphatidylinositol-mannosyltransferase I. *Mol Biol Cell* **16**, 1439–1448, doi:10.1091/mbc.e04-09-0802 (2005).
63. Martin, M. Cutadapt removes adapter sequences from high-throughput sequencing reads. *Embnet Journal* **17** (2011).
64. Li, W. *et al.* MAGeCK enables robust identification of essential genes from genome-scale CRISPR/Cas9 knockout screens. *Genome Biol* **15**, 554, doi:10.1186/s13059-014-0554-4 (2014).
65. Huang, Y. F. *et al.* Global mapping of glycosylation pathways in human-derived cells. *Dev Cell* **56**, 1195-1209 e1197, doi:10.1016/j.devcel.2021.02.023 (2021).
66. Branon, T. C. *et al.* Efficient proximity labeling in living cells and organisms with TurboID. *Nat Biotechnol* **36**, 880–887, doi:10.1038/nbt.4201 (2018).

Declarations

Acknowledgments

We thank Dr. Jean-François Dubremetz (Montpellier University) for the T5 4E10 mAb. We thank Drs. Hideki Nakanishi, Zijie Li, Ning Wang and Ganglong Yang for discussion and Yuki Uchikawa and Yuko Kabumoto for assistance with the cell sorting. We thank Keiko Kinoshita, Saori Umeshita, and Kae Imanishi for technical help. This work was supported by grants-in-aid from the National Natural Science Foundation of China (31900923, 31770853 and 32071278), Fundamental Research Funds for the Central

Universities (JUSRP121015), Program of Introducing Talents of Discipline to Universities (111-2-06), Japan Society for the Promotion of Science (JSPS) KAKENHI Grant 21H02415, Ministry of Education, Culture, Sports, Science and Technology (MEXT) of Japan KAKENHI Grant 17H06422, and a grant for Joint Research Project of the Research Institute for Microbial Diseases, Osaka University.

Author contributions

Y.-S.L., Y.W., M.F. and T.K. conceptualized and designed the study. Y.-S.L. and Y.W. conducted the experiments. Y.-S.L., X.Z., L.Z., S.-D. G. and Y.M. acquired and analyzed the data. Y.-S.L., M.F. and T.K. wrote the manuscript. All authors confirmed and edited the manuscript.

Competing interests

The authors declare no competing interests.

Correspondence and requests for materials should be addressed to M.F. and T.K.

Figures

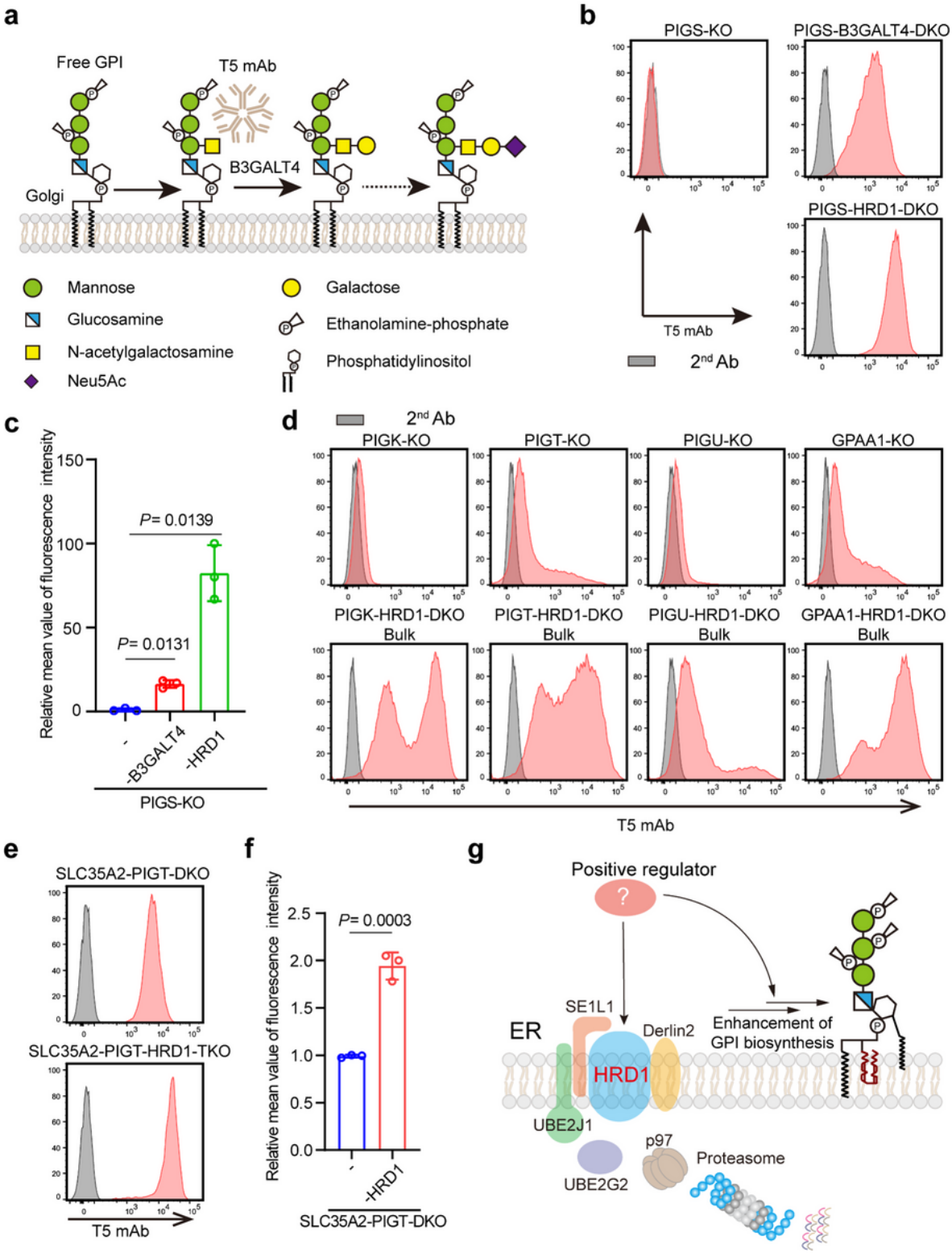

Figure 1

Defect in ERAD-L pathway upregulates GPI biosynthesis. a Schematic of free GPI side chain modifications with N-acetylgalactosamine (GalNAc), galactose, and salic acid. B3GALT4 is responsible for transferring galactose to the β1,4-linked GalNAc side chain of GPI. Monosaccharide symbols are drawn according to the symbol nomenclature for glycans. b and c Flow cytometry results for PIGS-B3GALT4-DKO and PIGS-HRD1-DKO cells stained with T5 mAb that recognizes free GPI with the GalNAc

side chain. The relative mean value of the fluorescence intensity of PIGS-KO was set to 1, and the relative intensity of free GPI in PIGS-B3GALT4-DKO and PIGS-HRD1-DKO cells is displayed as the mean ± SD from three independent experiments with p values (unpaired Student's t-test). d Flow cytometry results for pooled cultures of GPI transamidase subunit-defective cells, PIGK-KO, PIGT-KO, PIGU-KO, and GPAA1-KO after knocking out HRD1. Cells were stained with T5 mAb. e and f Flow cytometry analysis of SLC35A2-PIGT-DKO and SLC35A2-PIGT-HRD1-TKO cells stained with the T5 mAb. The relative mean value of the fluorescence intensity of SLC35A2-PIGT-DKO was set to 1, and the relative intensities of free GPI in SLC35A2-PIGT-DKO and SLC35A2-PIGT-HRD1-TKO cells are displayed as the mean ± SD from three independent experiments with p values (unpaired Student's t-test). g Schematic of the ERAD-L pathway negatively regulating GPI biosynthesis by degrading unknown factors. Validated genes are shown in the figure.

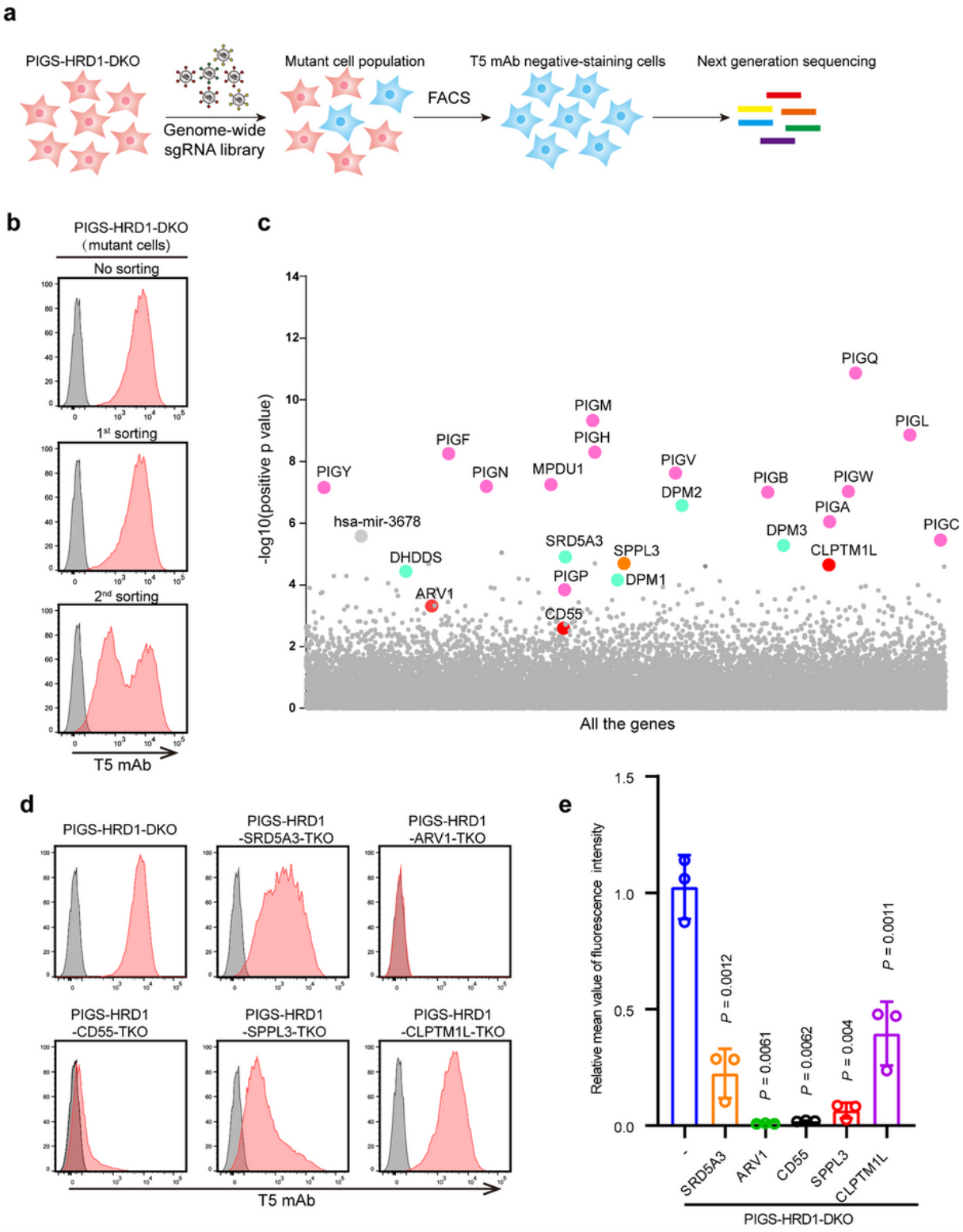

Figure 2

CRISPR–Cas9 pooled screening to identify regulators of GPI biosynthesis. a Strategy for a FACS-based genome-wide CRISPR screen in PIGS-HRD1-DKO cells. b Flow cytometry results for parental cells, 1st sorting, and 2nd sorting of PIGS-HRD1-DKO cells stained with T5 mAb. c Scatter plot showing genes corresponding to gRNAs that were significantly enriched in 2nd sorted PIGS-HRD1-DKO cells using model-based analysis of genome-wide CRISPR–Cas9 knockout (MAGeCK). The pink bubble denotes PIG genes,

the blue bubble denotes DPM-related and Dol-P-related genes, the yellow bubble denotes SPPL3, and the red bubble denotes functionally unknown genes in GPI biosynthesis. d and e Flow cytometry analysis of the knockout of top-ranking genes identified using our CRISPR screen in PIGS-HRD1-DKO cells. Cells were stained with T5 mAb. The relative mean value of the fluorescence intensity of PIGS-HRD1-DKO was set to 1, and the relative intensity of free GPI in knockout cells is displayed as the mean ± SD from three independent experiments with p values (unpaired Student's t-test).

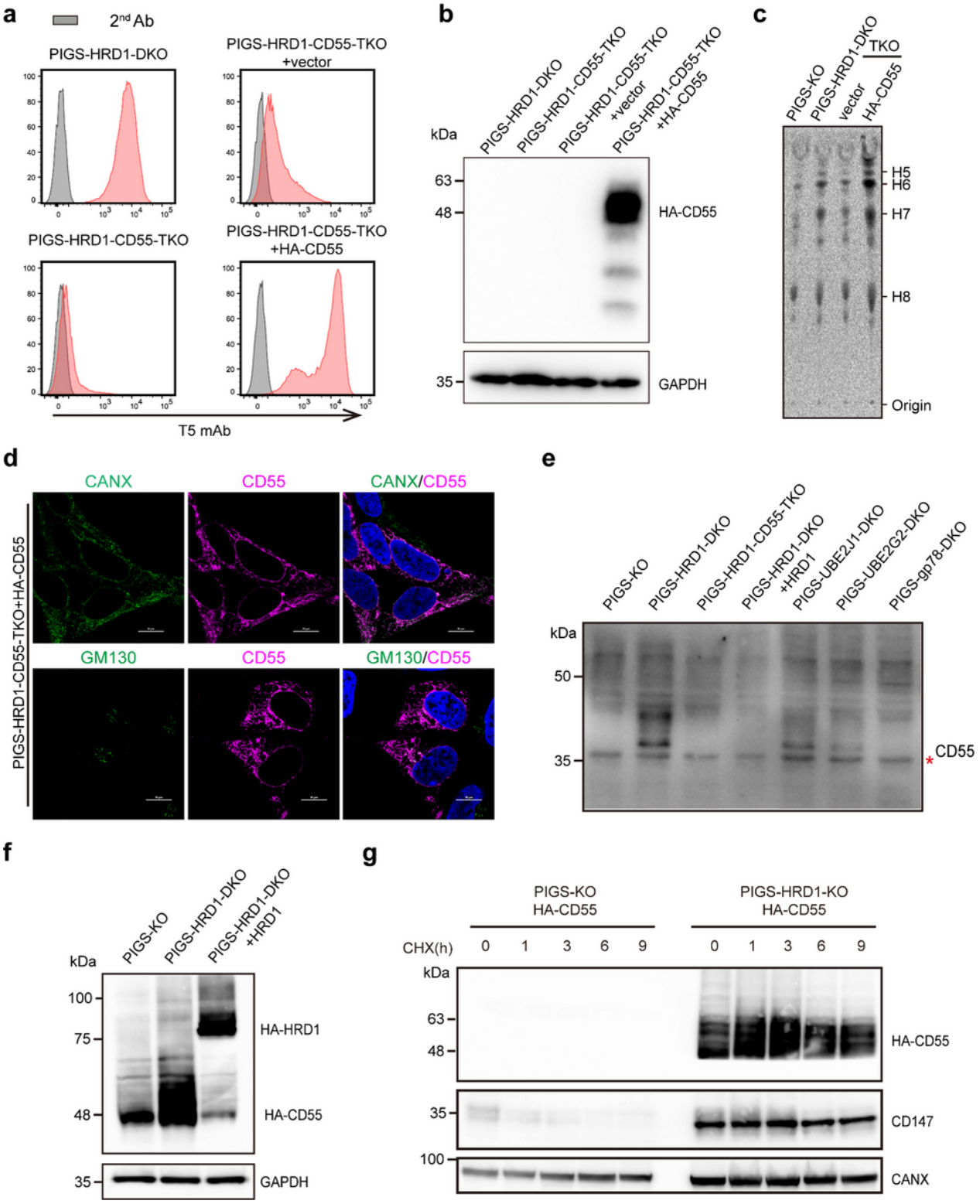

Figure 3

The precursor of CD55 regulates GPI biosynthesis and is a substrate of the ERAD-L pathway. a PIGS-HRD1-CD55-TKO cells were stably transfected with empty vector and HA-tagged CD55. Surface expression of free GPI was stained with T5 mAb and analyzed by flow cytometry. b Cell lysates prepared from the cells used in (a) were analyzed by western blotting. Expression of HA-CD55 was detected. GAPDH was used as a loading control. c GPI biosynthesis of the cells used in (a). d Fluorescence images of PIGS-HRD1-CD55-TKO cells stably expressing HA-tagged CD55. CANX, a marker of ER; GM130, a marker of cis-Golgi. Scale bar, 10 μm. e western blots of endogenous CD55. Lysates of PIGS-KO, PIGS-HRD1-DKO, PIGS-HRD1-CD55-TKO, PIGS-HRD1-DKO cells stably expressing HA-tagged HRD1, PIGS-UBE2J1-DKO, PIGS-UBE2G2-DKO, and PIGS-GP78-DKO cells were analyzed. The red asterisk indicates a nonspecific band. f Cell lysates prepared from PIGS-KO, PIGS-HRD1-DKO, and PIGS-HRD1-DKO cells stably expressing HA-tagged HRD1 transiently transfected with HA-tagged CD55 were analyzed by western blotting. Expression of HA-CD55 was detected. GAPDH was used as a loading control. g PIGS-KO and PIGS-HRD1-DKO cells stably expressing HA-tagged CD55 were treated with 1 μg/mL cycloheximide for 1 h, 3 h, 6 h, and 9 h. Cell lysates prepared from cycloheximide-treated cells were analyzed by western blotting. The protein amount of HA-CD55 was detected. CD147, a substrate of HRD1, was used as a positive control, and CANX was used as a loading control.

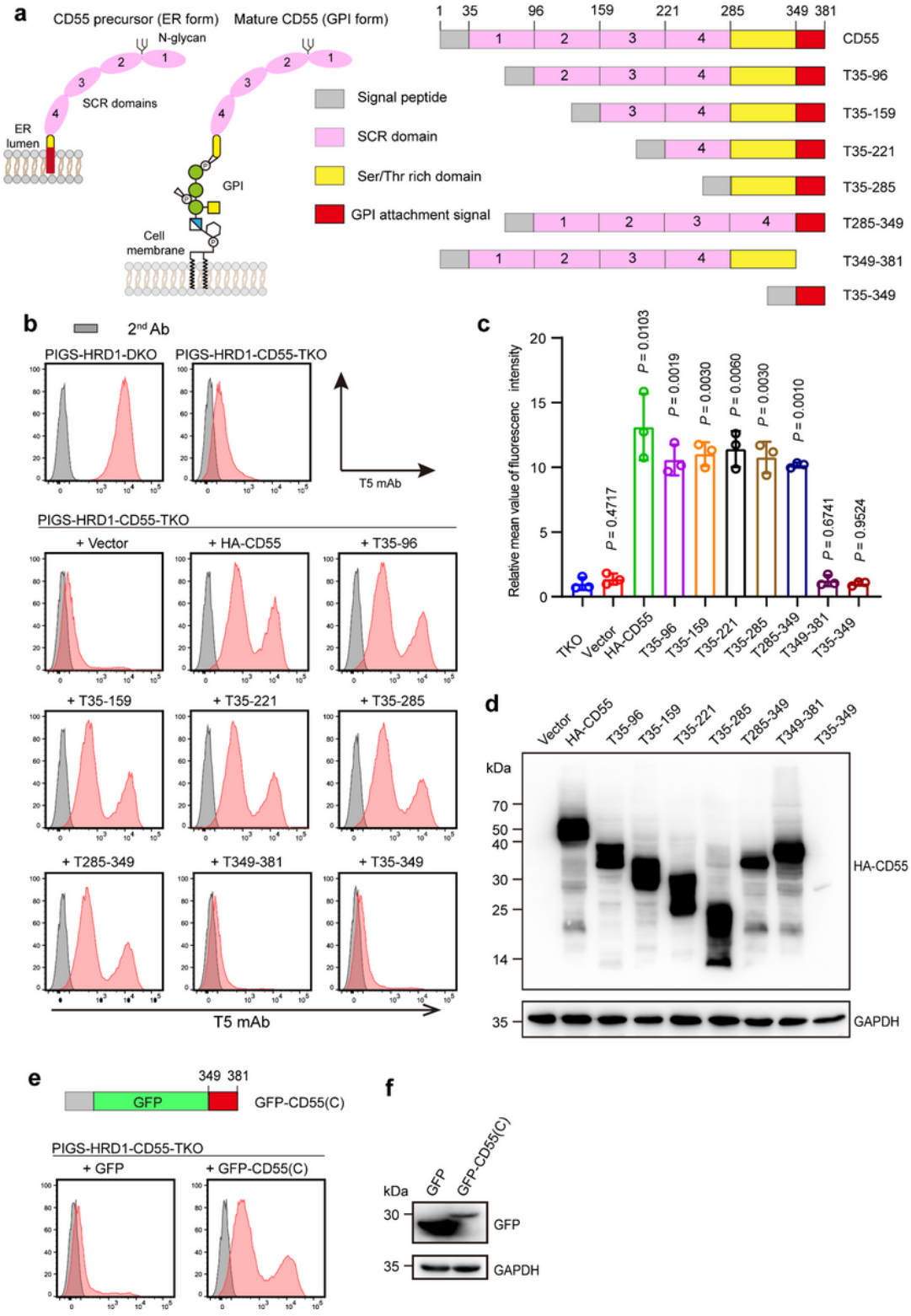

Figure 4

The GPI attachment signal peptide of CD55 regulates GPI biosynthesis. a Left: Schematic structure of the CD55 precursor (ER form) localized on the ER membrane, and mature CD55 (GPI form) localized on the cell surface. Right: Graphical depiction of the assay designs for truncated CD55 construction. Gray pane: Signal peptide; pink pane: SCR domain; yellow pane: Ser/Thr rich domain; red pane: GPI attachment signal. b and c Flow cytometry analysis of PIGS-HRD1-CD55-TKO cells transiently expressing plasmids

with different truncated CD55 variants. Cells were stained with T5 mAb. The relative mean value of the fluorescence intensity of PIGS-HRD1-CD55-TKO was set to 1, and the relative intensity of free GPI in transfected cells is displayed as the mean ± SD from three independent experiments with p values (unpaired Student's t-test). d Cell lysates prepared from the cells used in (b) were analyzed by western blotting. Expression of truncated CD55 variants was detected using HA antibody. GAPDH was used as a loading control. e and f The GPI attachment signal peptide of CD55 was fused with GFP and transiently expressed in PIGS-HRD1-CD55-TKO cells. GFP expressed plasmid was used as negative control. Cells were stained with T5 mAb and analyzed by flow cytometry. Cell lysates prepared from the cells used in (e) were analyzed by western blotting. The expression of fused proteins was detected by GFP antibody. GAPDH was used as a loading control.

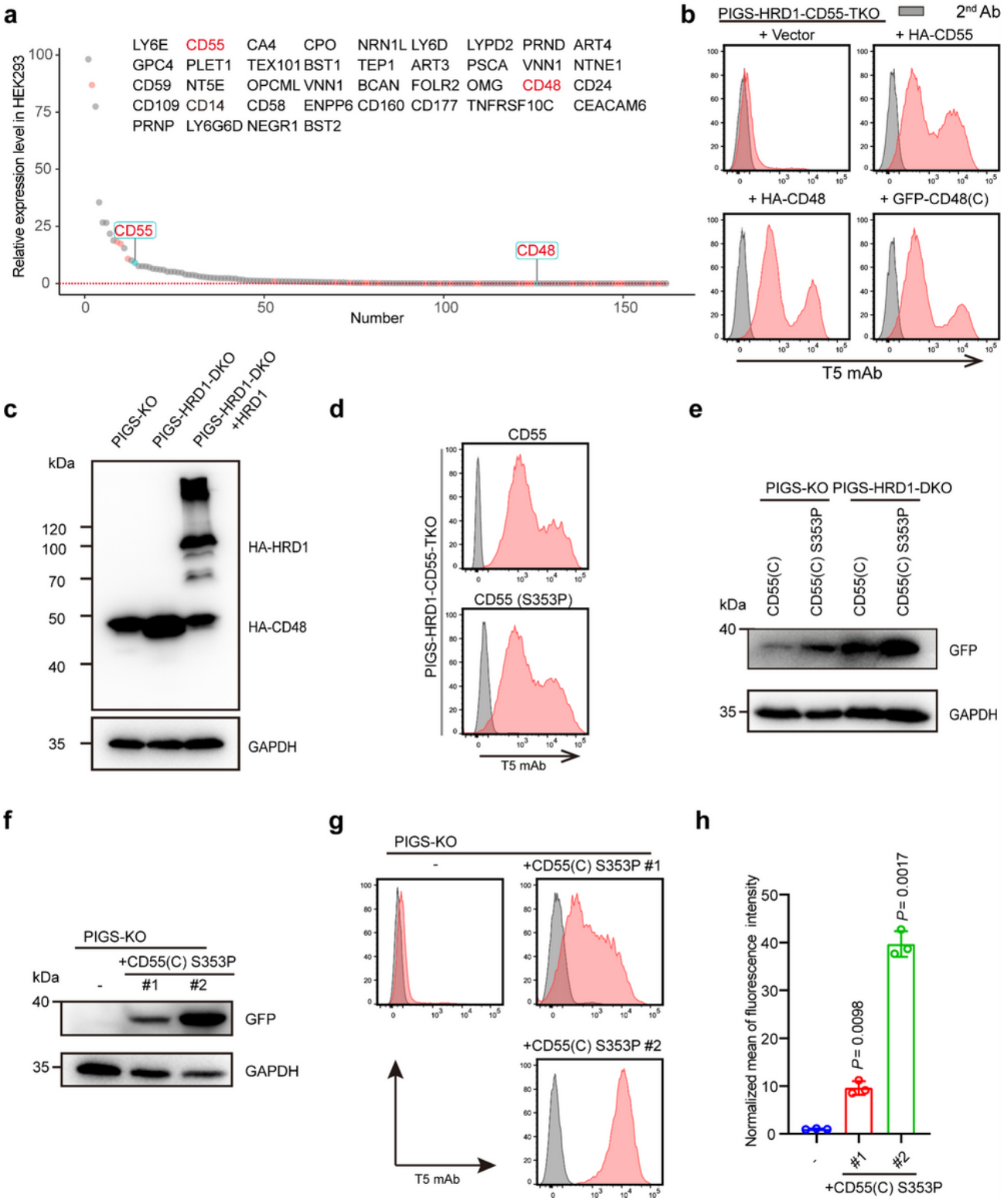

Figure 5

CD55 and CD48-dependent upregulation of GPI biosynthesis. a Relative levels of mRNAs for GPI-APs in HEK293 cells. Y axis: value of transcripts per million (TPM). X axis: number of GPI-APs. Red dot: GPI-APs chosen for knockout in PIGS-HRD1-DKO cells or overexpression in PIGS-HRD1-CD55-TKO cells. The names of the tested GPI-APs are listed. CD55 and CD48 are highlighted in red. b Flow cytometry analysis of PIGS-HRD1-CD55-TKO cells transiently expressing plasmids with HA-tagged CD55, CD48, GFP-fused

GPI attachment signal peptide of CD48 or empty vector. c Cell lysates prepared from PIGS-KO, PIGS-HRD1-DKO and PIGS-HRD1-DKO+HA-HRD1 rescued cells transiently expressing HA-CD48 were analyzed by western blotting. Protein expression was detected using the HA antibody. GAPDH was used as a loading control. d and e PIGS-HRD1-CD55-TKO cells were transiently transfected with constructs for expression of EGFP-fused wild-type CD55(C) or S353P CD55(C). The surface expression of free GPI was stained with T5 mAb and analyzed by flow cytometry. Cell lysates prepared from the cells transiently overexpressed EGFP-CD55(C) and S353P CD55(C) in PIGS-KO or PIGS-HRD1-DKO cells were analyzed by western blotting. f-h PIGS-KO cells were stably transfected with the GFP-fused CD55(C) S353P mutant, and two single clones, #1 and #2, were isolated. The expression of GFP-fused CD55(C) S353P was analyzed using western blotting (f). GAPDH was used as a loading control. g The surface expression of free GPI was stained with T5 mAb and analyzed by flow cytometry. h The relative mean value of the fluorescence intensity of PIGS-KO was set to 1, and the relative intensity of free GPI in clones #1 and #2 is displayed as the mean ± SD from three independent experiments with p values (unpaired Student's t-test).

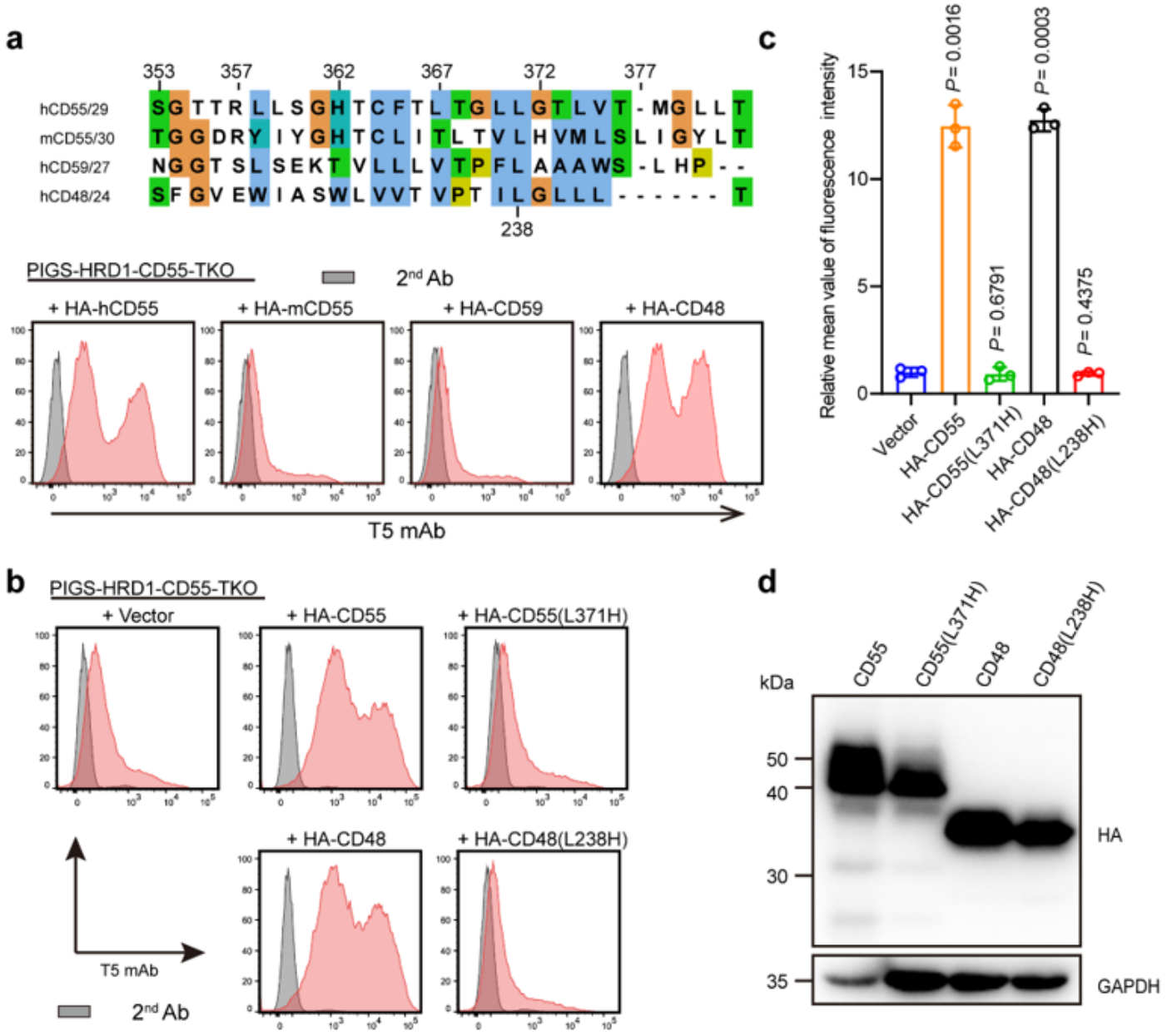

Figure 6

Exploration of the function important residues of the GPI attachment signal peptide in GPI biosynthesis. a Upper: GPI attachment signal peptides of human CD55, mouse CD55, CD59, and CD48 are aligned. The conservation of amino acids is shown in colors. Lower: Flow cytometry analysis of PIGS-HRD1-CD55-TKO cells transiently expressing plasmids with HA-tagged human CD55, mouse CD55, CD59, and CD48. Cells were stained with T5 mAb. b-d The indicated mutant CD55 and CD48 constructs were transiently expressed in PIGS-HRD1-CD55-TKO cells. Surface expression of free GPI was detected using flow cytometry. The relative mean value of the fluorescence intensity of PIGS-HRD1-CD55-TKO transfected empty vector was set to 1, and the relative intensity of free GPI in transfected cells is displayed as the mean ± SD from three independent experiments with p values (unpaired Student's t-test). Cell lysates prepared from the cells used in (b) were analyzed by western blotting. The expression of fused proteins was detected by HA antibody. GAPDH was used as a loading control.

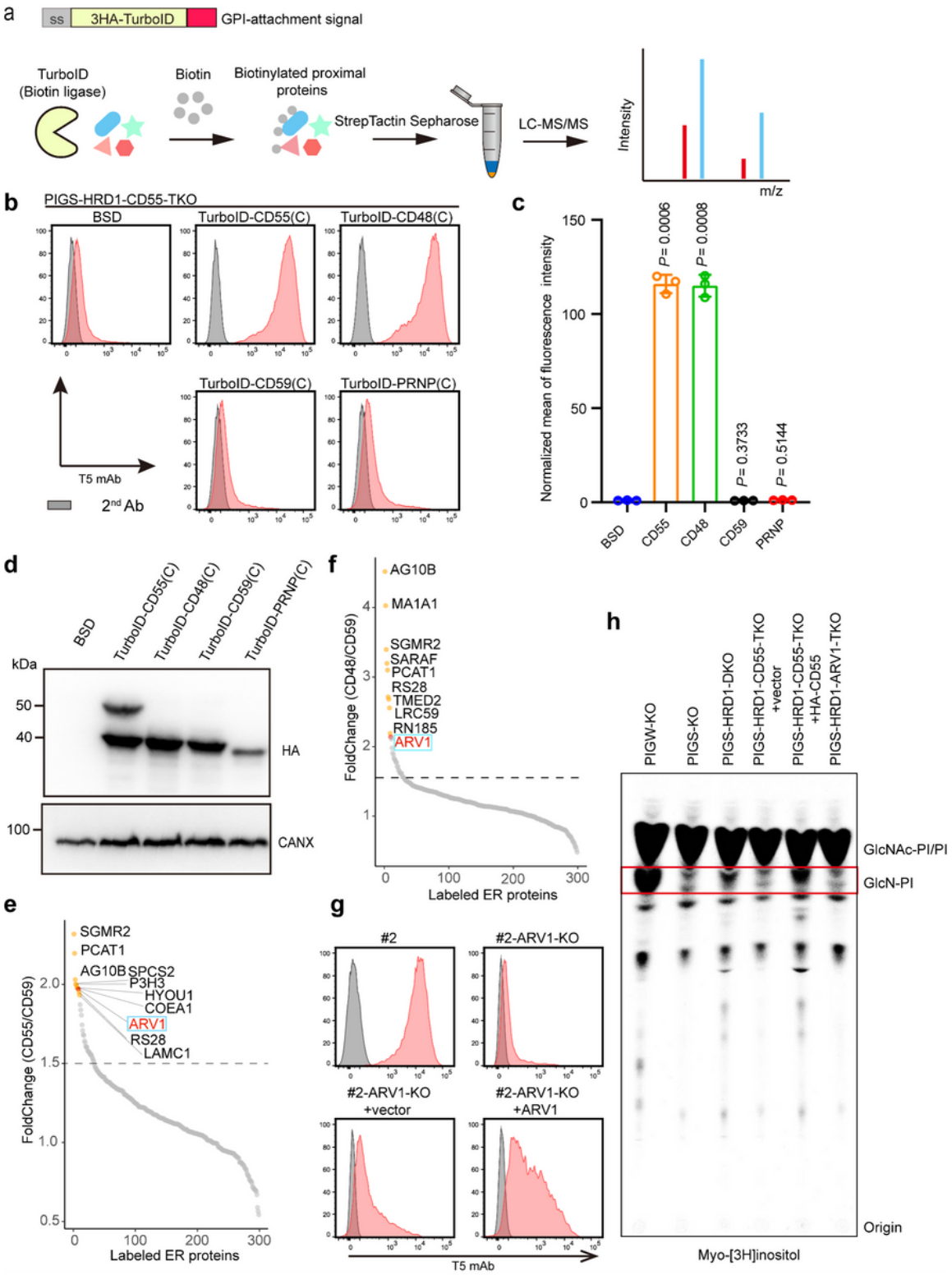

Figure 7

Proximity labeling identified ARV1 as spatially close and functionally similar to CD55. a Schematic strategy of biotin labeling and MS-based protein identification. A 3x HA-tagged biotin ligase (Turbo-ID) was fused with the GPI attachment signal peptide. b-d PIGS-HRD1-CD55-TKO cells were stably transfected with empty vector and 3x HA-tagged GPI attachment signal peptides of the CD55, CD48, CD59, and PRNP. The surface expression of free GPI was stained with T5 mAb and analyzed by flow

cytometry. The relative mean value of the fluorescence intensity of PIGS-HRD1-CD55-TKO transfected empty vector was set to 1, and the relative intensity of free GPI in related cells is displayed as the mean ± SD from three independent experiments with p values (unpaired Student's t-test). Cell lysates prepared from the cells used in (b) were analyzed by western blotting. The expression of fused proteins was detected using the HA antibody. CANX was used as a loading control. e The fold change in TurboID-CD55(C) versus TurboID-CD59(C) biotin and TMT-labeled peptide. A fold change ranking at top ten is highlighted in orange, and ARV1 is highlighted in red. f The fold change in TurboID-CD48(C) versus TurboID-CD59(C) biotin and TMT-labeled peptide. A fold change ranking at top ten is highlighted in orange, and ARV1 is highlighted in red. g Flow cytometry of CD55(C) S353P-expressing PIGS-KO cells (clone #2), ARV1-KO clone #2 cells, and ARV1-KO clone #2 cells transiently transfected with empty vector and plasmid containing 3x Flag-tagged ARV1. Cells were stained with T5 mAb. h HPTLC analysis of GlcN-PI from cells metabolically labeled with [3H] inositol for 24 h.

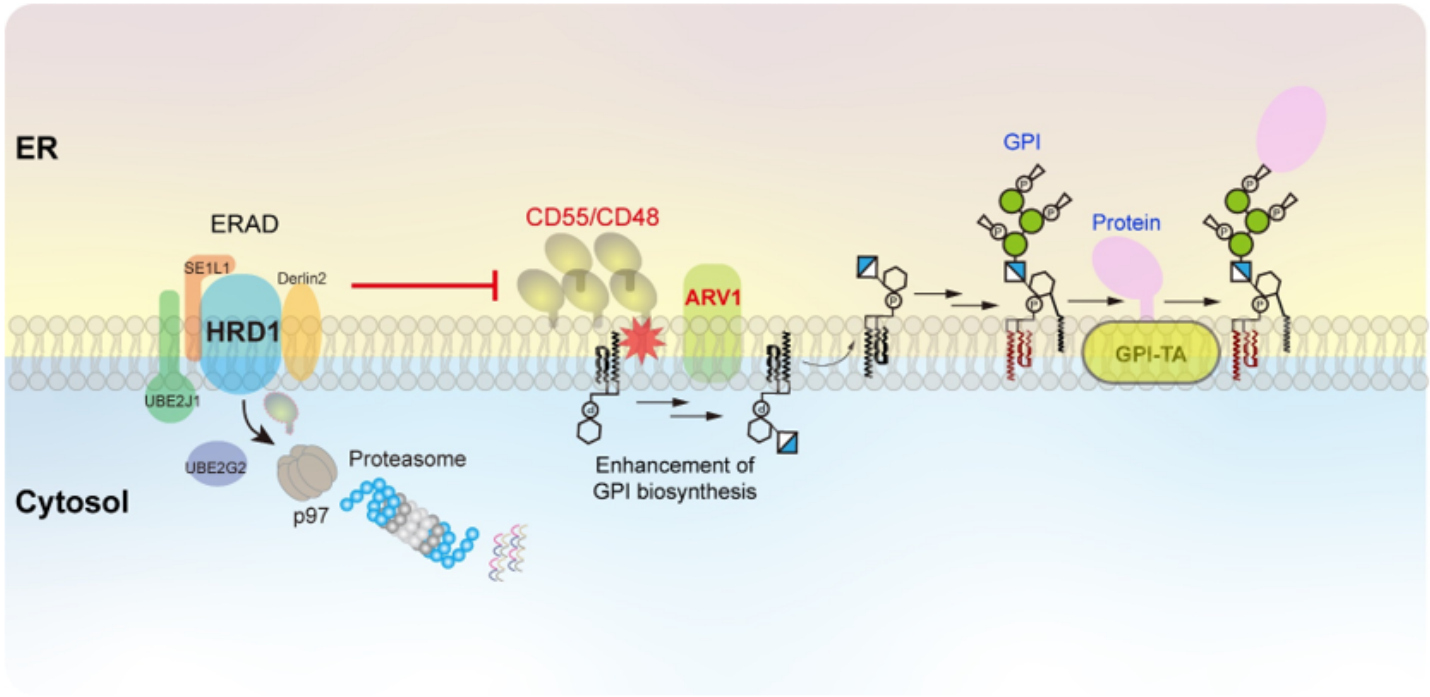

Figure 8

Schematic model of the functional roles of the HRD1-dependent ERAD-L substrate CD55 in regulating GPI biosynthesis. CD55 or CD48 precursor proteins are processed and transferred to GPI by the GPI transamidase, generating GPI-anchored forms. Conversely, these precursor proteins that failed to have GPI attachment are degraded normally through the HRD1-dependent ERAD-L pathway. Once the ERAD-L pathway is impaired, CD55 and CD48 precursor proteins accumulate in the ER, in turn upregulating GPI biosynthesis at early step(s). ARV1 is critical for the upregulation of GPI biosynthesis under CD55/CD48 accumulated conditions.

Supplementary Files

This is a list of supplementary files associated with this preprint. Click to download.

- DescriptionofSupplementaryFiles.docx
- SupplementaryData1.xlsx
- SupplementaryData2.xlsx
- SupplementaryData3.xlsx
- SupplementaryData4.xlsx
- SupplementaryData5.xls
- SupplementaryFigures.docx